Computer Assisted Mechanics and Engineering Sciences, 9: 239–269, 2002.

Heat transmission across fouled tubes analysed by Trefftz approach

Teodor Skiepko
Faculty of Mechanics, Dept. of Thermodynamics and Fluid Mechanics, Białystok Technical University, ul. Wiejska 45C, 15-351 Białystok, Poland

(Received September 28, 2000)

The paper presents application of the Trefftz method for analysis a case of heat conduction problem across two coupled regions – fouling layer of complex form deposited onto the tube wall at its outer periphery. Taken into considerations modes of heat transfer from a hot gas to the outer surface of the fouling layer are: either by pure convection or radiation, and by both the modes combined. A fluid flowing inside the tube exchanges heat by only convection at constant transfer coeffcient. Based on the variational principle and Trefftz method the boundary weighted residual approach has been developed providing in turn an equation system for analysis of the problem under study. Then, results of series of systematic numerical experiments illustrating convergence and accuracy of the approach when applied to the case in point have been shown for a specific input data set assumed. To emphasise practical significance of the method, a calculated temperature distribution 3D chart and thermal resistance of 2D fouling deposits conclude the paper.

NOMENCLATURE

$\mathrm{d}s$	– arc differential,
E_0 , E_1 , C_n , c_n , D_n , d_n	– coefficients in formule describing temperature in the fouling layer,
F_0 , F_1 , A_n , a_n , B_n , b_n	– coefficients in formule describing temperature in the tube metal,
J	– functional,
k_f	– foulant thermal conductivity,
k_m	– tube metal thermal conductivity,
$k = k_f/k_m$	– thermal conductivity ratio,
M	– number of trigonometric terms,
N	– outward normal vector,
Δq	– flue gas-heated fluid heat transfer imbalance,
$\dot{Q}$	– heat rate,
r, φ	– variables of cylindrical coordinate system,
r_f	– radial coordinate at boundary of fouling layer,
r_2	– inner tube radius,
r_o	– outer tube radius,
R	– specific thermal resistance,
tol	– convergence accuracy,
T, t	– temperature, [K] or [deg. Celsius], respectively,
U	– overall heat transfer coeeficient,

Greek symbols

α	– surface heat transfer coefficient,
$\alpha(\varphi)$	– nonuniform α,
$\bar{\alpha}$	– mean value of α,

Γ_f – outer boundary of fouling layer,
δ_n – defined by Eq. (A20)
ε – emissivity,
Δ – error in boundary conditions,
$\theta_f = T_f/T_1$ – dimesionless foulant temperature,
$\theta_m = (T_m - T_2)/(T_1 - T_2)$ – dimesionless tube temperature,
$\Theta = T_2/T_1$ – heated fluid to flue gas temperature ratio.
$\Theta_1 = T_1/(T_1 - T_2)$ – flue gas to driving force temperature ratio,
$\Theta_2 = T_2/(T_1 - T_2)$ – heated fluid to driving force temperature ratio,
κ – defined by Eq. (A14)
$\rho = r/r_2$ – dimensionless radial coordinate,
$\rho_o = r_o/r_2$ – dimensionless outer tube radius,
σ_o – Stefan–Boltzmann constant,
$\psi(\rho, \varphi)$ – trial functions,
Ω_f – fouling layer region.

Dimensionless numbers

$Bi_2 = \alpha_2 r_2/k_m$ – Biot number at heated fluid–tube metal boundary,
$Bi_r = 5.67 \cdot 10^{-8} \cdot \frac{\varepsilon_f + 1}{2} \varepsilon_1 T_1^3 r_o/k_f$ – Biot number under radiation mode at flue gas–fouling layer boundary,
$Bi_c = \alpha_c r_o/k_f$ – Biot number under convection mode at flue gas–fouling layer boundary.

Subscripts

c – convection,
cl – clean,
f – fouled or fouling layer, where appropriate,
m – tube metal,
N – nonuniform,
r – radiation,
U – uniform,
1 – refers to flue gas,
2 – refers to heated medium.
3,4,5,6 – refers to boundary condition (3), (4), (5), (6), respectively.

1. Introduction

Although transport processes in heat exchangers attract permanent attention paid by investigators, most of the efforts concern heat-flow phenomena at so called "clean conditions" when no undesired fouling deposit exists at the heat transfer surface. Thus, much the results achieved have applications in heat transfer engineering significantly limited because the fouling can contribute markedly to the total resistance for heat flow. In common use, one dimensional (1D) modeling is applied for heat transmission process across a fouled tube. Consequently, deteriorate effect of the fouling is included by means of two additional terms of the thermal resistance meaning, being referred as the fouling factors at the heated and cooled surface of the exchanger wall, respectively. The terms supplement sum all the individual thermal resistances in the path of heat flow between the fluids.

However, there are a lot of practical cases where the foulant deposit is nonuniform in its shape around the tube periphery. Typical exemplary cases refer to the unburned mineral content of fossil

fuels carried as the fly ash in form of small particles suspended in the flue gas stream. Some of the particles when approaching the heat transfer surface of a boiler tube can be bounced off and some can stick. Due to that a sort of mineral deposit is accumulated on the tubes as an undesired fouling layer, in general, of nonuniform thickness. In Fig. 1 several pictures demonstrating shapes of the deposit are shown as found in the literature.

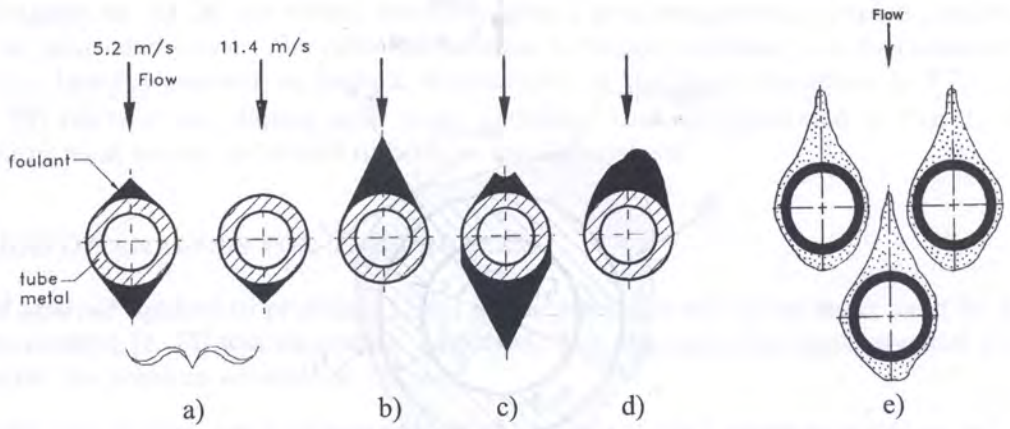

Fig. 1. Shapes of fouling layer (see description in the text) on the outer surface of the boiler tubes (note: proportions between dimensions of the tube and fouling layers are preserved)

In Fig. 1a two shapes of the fouling layer on a staggered tube bank observed during laboratory investigations [4] are shown. Fouling as in Fig. 1b has been observed [7] on tubes of a steam reheater. In Fig. 1c a complex fouling shape found on a tube of a bituminous-estonian-shale-fired boiler [5] is presented. For a brown-coal-fired boiler the slag type fouling [14] of the primary superheater flown around by flue gas of temperature 1100–1200 °C is given in Fig. 1d, where it can be seen that the deposit shape is markedly unsymmetrical with respect to direction of the overall inflow. Deposit shapes shown in Fig. 1e refer to a foulant on tubes of a staggered bank in a zone of lower temperatures of a residual-oil-fired boiler [1].

The pictures show that shape of the fouling layer can be of a complex form which thickness is essentially nonuniform, ranged practically from zero to about the tube diameter. Taking into account that the thermal conductivity of the foulant material is rather low (roughly about $\sim 1\%$ of that for the tube metal) one can expect significant nonuniformities in temperature distribution along outward circumference of the fouling layer. Consequently, the problem becomes two-dimensional (2D). A search in the literature did not reveal any prior treatment such the heat transfer problem across a nonuniformly fouled wall. It has motivated to develop a methodology for study the problem as well as to conduct investigations on how the nuniformity can affect the transfer of great practical significance for engineering.

2. Modelling of heat transfer process across a fouled boiler tube

Consider a cross-section of a boiler tube covered on the outer periphery with nonuniform (around the tube) fouling layer of arbitrary given shape. Heat is transferred under a steady state process across the fouled tube wall from the flue gas into a heated medium flowing inside the tube. The convection and radiation modes of heat transmission at the outer surface of the fouling layer are included into the analysis by means relevant surface heat transfer coefficients, which circumferential variations are also taken into account. Medium flowing inside the tube exchanges heat by convection at a constant transfer coefficient from the inner tube surface that is clean. No thermal contact resistance is asssumed to occur at the "tube–fouling layer" interface. All the physical properties used in the analysis are independent of position and temperature both for the tube metal and

foulant material. More, temperatures of the flue gas and heated medium are constant in the vicinity of a considered cross-section of the tube. Figure 2 depicts the coordinate system applied in the analysis and a schematic of the fouled tube in which the tube metal region is ranging from $r = r_2$ to $r = r_o$ and fouling layer from $r = r_o$ to $r = r_f$.

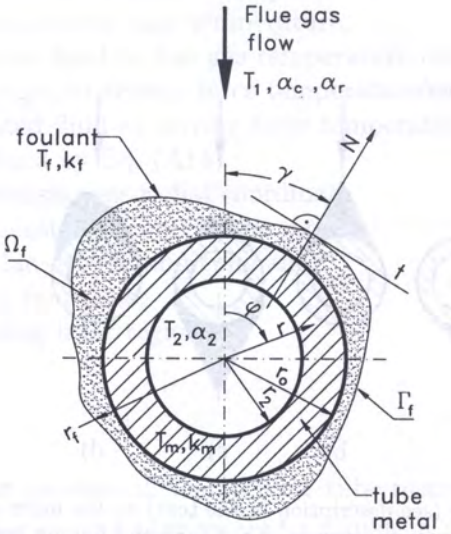

Fig. 2. Assumed coordinate system for analysis of heat transfer from a hot flue gas at T_1 to a cold fluid at T_2 across a tube wall covered with outer fouling layer

Based on assumptions as specified above and taking into account dimensionless parameters defined in Section 4.1 and Nomenclature one can arrive at the following nondimensional governing equations emboding energy balances:

- for the fouling layer

$$\nabla^2 \theta_f = 0, \tag{1}$$

- for the tube metal

$$\nabla^2 \theta_m = 0. \tag{2}$$

Equations (1)–(2) subject to relevant boundary conditions describing transfer of heat across boundaries of the tube metal and fouling layer:

- heat transmission at convection heat transfer coefficient α_2 from the inner surface ($\rho = 1$) of the tube into a fluid at temperature T_2,

$$\left.\frac{\partial \theta_m}{\partial \rho}\right|_{\rho=1} - Bi_2\, \theta_m|_{\rho=1} = 0, \tag{3}$$

- continuity both the temperature and heat flux at the "tube–fouling layer" interface ($\rho = \rho_o$),

$$\theta_m|_{\rho=\rho_o} + \Theta_2 = \Theta_1 \theta_f|_{\rho=\rho_o}, \tag{4}$$

$$\left.\frac{\partial \theta_m}{\partial \rho}\right|_{\rho=\rho_o} = k\Theta_1 \left.\frac{\partial \theta_f}{\partial \rho}\right|_{\rho=\rho_o}, \tag{5}$$

- heat transmission, at convection α_c and radiation α_r heat transfer coefficients when combined as $\alpha_c + \alpha_r$, from the flue gas at temperature T_1 into the outer boundary of the fouling layer Γ_f,

$$\left.\frac{\partial \theta_f}{\partial N}\right|_{\Gamma_f} + \frac{1}{\rho_o}\left[Bi_c \cdot \theta_f + Bi_r \cdot \theta_f^4\right]\Big|_{\Gamma_f} = \frac{1}{\rho_o}[Bi_c + Bi_r]. \tag{6}$$

Model equations (1)–(6) describe a two-dimensional nonhomogeneous coupled boundary-value problem for heat conduction. The problem becomes a strong nonlinear, due to radiation transfer coeffcient α_r being dependent on foulant temperature at the outer boundary as $T_f^4|_{r=r_f}$. More, condition (6) refers to the fouling layer outer periphery that, as illustrated in Fig. 1, can be of complex form what makes additional difficulties for the analysis.

3. Method of analysis for the problem

Method of analysis applied to problem (1)–(6) in the present study, is the same as in [8, 11] where the Trefftz method [2, 13] was succesfully employed. The approach has some essential advantages preferable for the problem studied, as follows:

- solution of the problem can be obtained through analysis of small algebraic equation sets resulting in explicit formulae of high accuracy ready to determine temperature distributions throughout the whole region of the tube metal and fouling layer, respectively,
- it does not need any grid or mesh, thus, problems of subdividing the two-dimensional complex coupled region of the interest by discrete points or elements falls off as well as further mesh refinement, therefore, the method is especially useful for the problem in point because temperature gradients across the fouling deposit can be of several orders different than those across the tube metal due to great difference in the thermal conductivities,
- it does work well when applied to solve strong nonlinear problems of radiation heat transfer because analysis can be performed through small sets of nonlinear equations,
- analysis is performed using boundary conditions that, in general, are of less complex than governing equations related to.

3.1. The variational problem

The following forms have been assumed for expressions describing temperature fields:

- in the fouling layer

$$\theta_f(\rho, \varphi) = \sum_{n=1}^{n=K} \lambda_n \psi_n(\rho, \varphi), \tag{7}$$

- in the tube metal

$$\theta_m(\rho, \varphi) = \sum_{n=1}^{n=K} \mu_n \psi_n(\rho, \varphi), \tag{8}$$

where, by virtue of the Trefftz method we apply here, trial functions $\psi_n(\rho, \varphi)$ must be selected as particular linearly independent solutions of governing Eqs. (1) and (2), respectively. Thus, the following solutions have been chosen: $\psi_1(\rho, \varphi) = 1$, $\psi_2(\rho, \varphi) = \ln \rho$, $\psi_n(\rho, \varphi) = \rho^n \cos n\varphi$, $\psi_n(\rho, \varphi) = \rho^{-n} \cos n\varphi$, $\psi_n(\rho, \varphi) = \rho^n \sin n\varphi$, $\psi_n(\rho, \varphi) = \rho^{-n} \sin n\varphi$. Consequently, Eqs. (7) and (8) can be constructed in the forms:

- for the fouling layer

$$\theta_f(\rho,\varphi) = E_0 + E_1 \ln\rho + \sum_{n=1}^{n=M} \rho^n (C_n \cos n\varphi + c_n \sin n\varphi) + \sum_{n=1}^{n=M} \rho^{-n} (D_n \cos n\varphi + d_n \sin n\varphi), \tag{9}$$

- for the tube metal

$$\theta_m(\rho,\varphi) = F_0 + F_1 \ln\rho + \sum_{n=1}^{n=M} \rho^n (A_n \cos n\varphi + a_n \sin n\varphi) + \sum_{n=1}^{n=M} \rho^{-n} (B_n \cos n\varphi + b_n \sin n\varphi). \tag{10}$$

Unknown coefficients F_0, F_1, E_0, E_1, A_n, a_n, B_n, b_n, C_n, c_n, D_n, d_n, where $n = 1, \ldots, M$, must be determined in such a way that Eqs. (9) and (10) subject to satisfy boundary conditions (3)–(6). Therefore, solutions (9) and (10) when substituted into conditions (3)–(5) give expressions relating coefficients F_0, F_1, A_n, a_n, B_n, b_n of Eq. (10) to coefficients E_0, E_1, C_n, c_n, D_n, d_n shown in Eq. (9) – see Appendix A for details. Thus, Eq. (9) describing temperature distribution in the fouling layer can be rearranged to be given as

$$\theta_f(\rho,\varphi) = \Theta + [\kappa + \ln\rho]E_1 + \sum_{n=1}^{n=M} (\rho^n - \rho^{-n}\delta_n)(C_n \cos n\varphi + c_n \sin n\varphi). \tag{11}$$

Note, Eq. (11) does not fulfil yet condition (6). For the case in point, steady state heat conduction equation (1) when accompanied by boundary condition (6) is equivalent to the condition of extremum for the following functional (for the problem considered see derivation in [8, 11], fudamentals in [2, 13])

$$J\langle\theta_f\rangle = \frac{1}{2}\iint_{\Omega_f} (\operatorname{grad}\theta_f)^2 \,\mathrm{d}\Omega_f + \frac{1}{2\rho_o}\int_{\Gamma_f} \left\{ Bi_c\theta_f^2 + \frac{2}{5}Bi_r\theta_f^5 - 2[Bi_c + Bi_r]\theta_f \right\} \mathrm{d}s. \tag{12}$$

Therefore, the variational principle will be used to determine coefficients E_1, C_n and c_n in Eq. (11) taking into account condition (6).

3.2. Construction of the boundary weighted residual approach

To derive the equation system determining unknown coefficients E_1, C_n and c_n, $n = 1, \ldots, M$, we substitute now Eq. (11) into functional (12). In turn, the functional becomes a function of many variables with respect to the unknown coefficients. Then, based on condition of the extremum for functional (12) with constrains defined by Eqs. (A10)–(A11), (A15)–(A21) and taking into account that Eq. (11) selected for θ_f, by virtue of the Trefftz approach applied here, satisfies the Laplace equation $\nabla^2\theta_f = 0$, we can construct finally the following equation system from which coefficients E_1, C_n and c_n, $n = 1, \ldots, M$ can be determined

$$\left.\begin{aligned} &\int_{\Gamma_f} X(\theta_f)\,(\kappa + \ln\rho)\,\mathrm{d}s = 0, \\ &\int_{\Gamma_f} X(\theta_f)\,(\rho^n - \rho^{-n}\delta_n)\cos n\varphi\,\mathrm{d}s = 0, \\ &\int_{\Gamma_f} X(\theta_f)\,(\rho^n - \rho^{-n}\delta_n)\sin n\varphi\,\mathrm{d}s = 0, \\ &n = 1, \ldots, M, \end{aligned}\right\} \tag{13}$$

where

$$X(\theta_f) = \rho_o \frac{\partial \theta_f}{\partial N} + Bi_c \theta_f + Bi_r \theta_f^4 - [Bi_c + Bi_r] \tag{14}$$

and θ_f is assumed to be given by Eq. (11). Note that, with respect to condition (6), equations system (13) keeps the weighted residual form [3] of the Galerkin formulation, where $(\kappa + \ln\rho)$, $(\rho^n - \rho^{-n}\delta_n)\cos n\varphi$, and $(\rho^n - \rho^{-n}\delta_n)\sin n\varphi$ are the weighting functions. In turn, the boundary weighted residual approach is applied to solve the problem under study.

After substitution of $\mathrm{d}s = \sqrt{\rho_f^2(\varphi) + (\mathrm{d}\rho_f(\varphi)/\mathrm{d}\varphi)^2}$ for the linear element in system (13) and performing necessary integrations, where appropriate, one obtains a nonlinear equation system with respect to unknown coeffictients E_1, C_n and c_n, $n = 1, \ldots, M$. The coeffcients when found and substituted into expressions (A10), (A11), (A15)–(A21) yield coefficients F_0, F_1, A_n, a_n, B_n, and b_n, used in Eq. (10) applied to determine temperature in the tube wall.

Equation (10) represents of $4M + 2$ and Eq. (11) of $2M + 1$ unknowns for established $n = M$. In addition, coefficients E_0, D_n, d_n in Eq. (9) represent of $2M + 1$ unknowns, thus a total number of unknowns to be determined for the problem is $8M + 4$. The number of equations being at the disposal is:

- for unknowns E_1, C_n, c_n: $2M + 1$ equations of system (13),
- for unknowns F_0, F_1, A_n, a_n, B_n, b_n: 2 equations, (A10), (A11), and $4M$ equations, (A15)–(A18),
- for unknowns E_0, D_n, d_n: 1 equation, (A12), and $2M$ equations, (A19), (A21).

Thus, a total of $8M+4$ linear/nonlinear equations are also available to determine $8M+4$ unknowns mentioned above. Consequently, problem of finding the coefficients is well closed. The computational procedure for finding the coefficients consists in the following consecutive steps:

- solving equations system (13) to determine coefficients E_1, C_n, c_n, $n = 1, \ldots, M$,
- knowing E_1 we calculate coefficients: F_0, F_1, E_0 using Eqs. (A10), (A11) and (A12), respectively,
- then based on (A20) factor δ_n for $n = 1, \ldots, M$, and coeffcients D_n, d_n, $n = 1, \ldots, M$, are calculated using Eqs. (A19) and (A21),
- having now coeffcients C_n, c_n, D_n, d_n, $n = 1, \ldots, M$, we use Eqs. (A15)–(A18) to calculate A_n, a_n, B_n, b_n, $n = 1, \ldots, M$,
- because all the required coeffcients have been determined Eq. (10) is ready to calculate temperature in the tube metal domain and Eqs. (9) or (11) work for temperature distribution in the fouling layer.

4. Numerical experiments

The experiments performed were aimed:

- at first, to estimate convergence and accuracy of the computational strategy developed,
- at the second, to obtain some results for possible applications in engineering.

All the numerical experiments were carried out using an input data set assumed as for a boiler tube of the superheater.

4.1. Assumed input data describing heat transfer conditions

The following input data for the numerical experiments reported in the present study have been used:

- *fluid temperatures*:

  flue gas: $T_1 = 1198.0$ K,
  heated fluid: $T_2 = 768.0$ K.

- *convection heat transfer coeffcient*:

  flue gas side:
  mean value: $\bar{\alpha}_c = 48.90$ [W/(m^{2}K)],
  nonuniform value: $\alpha_c(\varphi) = 48.90 \cdot (1.0 + 0.41\cos\varphi + 0.25\cos 2\varphi)$ [W/(m^{2}K)],
  heated fluid side, mean value: $\bar{\alpha}_2 = 4280.0$ [W/(m^{2}K)],

- *radiation heat transfer coeffcient* (only on the flue gas side):

$$\alpha_r = 5.67 \cdot 10^{-8} \frac{\varepsilon_f + 1}{2} \varepsilon_1 \frac{T_1^4 - T_f^4}{T_1 - T_f}, \text{ [W/(m}^2\text{K)]},$$

  where it has been assumed that $\varepsilon_f = 0.80$, and $\varepsilon_1 = 0.44$,

- *thermal conductivity*:

  foulant material: $k_f = 0.20$ [W/(mK)],
  tube metal: $k_m = 23.30$ [W/(mK)].

The dimensionless parameters for problem (1)–(6), determined taking into account the above heat transfer conditions are:

- *Biot numbers*:

$$Bi_2 = \frac{\alpha_2 r_2}{k_m} = 2.2043,$$

$$Bi_r = 5.67 \cdot 10^{-8} \frac{\varepsilon_f + 1}{2} \varepsilon_1 T_1^3 \frac{r_o}{k_f} = 3.6675,$$

$$Bi_c = \bar{\alpha}_c \frac{r_o}{k_f} = 4.6455, \quad \text{using mean value of the convection heat transfer coeffcient,}$$

$$Bi_c = \alpha_c(\varphi) \frac{r_o}{k_f} = 4.6455 + 1.9047\cos\varphi + 1.1614\cos 2\varphi, \quad \text{when coeffcient } \alpha_c(\varphi) \text{ is nonuniform,}$$

- *other parameters*:

$$\Theta_1 = \frac{T_1}{(T_1 - T_2)} = 2.7860, \qquad \Theta_2 = \frac{T_2}{(T_1 - T_2)} = 1.7860, \qquad \Theta = \frac{T_2}{T_1} = 0.64107.$$

$$\rho_o = \frac{r_o}{r_2} = 1.5833, \qquad k = \frac{k_f}{k_m} = 8.5837 \cdot 10^{-3},$$

Note that the symmetry of fouled tubes with respect to direction of the overall flue gas inflow results in that coefficients a_n, b_n in Eq. (10) and coeffcient c_n in Eq. (11) must vanish for $n = 1, \ldots, M$. Consequently, for the symmetrical cases equations system (13) can be reduced to

$$\left.\begin{aligned} &\int_{\Gamma_f} X(\theta_f)\,(\kappa + \ln\rho)\,\mathrm{d}s = 0, \\ &\int_{\Gamma_f} X(\theta_f)\,(\rho^n - \rho^{-n}\delta_n)\cos n\varphi\,\mathrm{d}s = 0, \end{aligned}\right\} \tag{15}$$

where $n = 1, \ldots, M$, and temperature distribution throughout the fouling layer is described by

$$\theta_f(\rho, \varphi) = \Theta + [\kappa + \ln \rho] E_1 + \sum_{n=1}^{n=M} C_n(\rho^n - \rho^{-n}\delta_n) \cos n\varphi. \tag{16}$$

4.2. Method of analysis for the boundary weighted residual equation system

Equations system (15) is a nonlinear when radiation contributes in heat transport. Applied here method of solving for the system is an iterative Newton–Raphson [1] – see Appendix B for a short description. Because of complexity of the expressions involved into equations system (15) a computer code has been prepared to solve this system and thoroughly checked for convergence and accuracy. Some preliminary results obtained by the code showed that the double precision technique programming is desired such that it has been used in the code.

Convergence criteria

Regarding the convergence accuracy *tol*, preliminary numerical trials performed in the study with decreasing values of *tol* showed that its values do affect the results if $tol \geq 1.0 \cdot 10^{-13}$. Consequently, the convergence accuracy was assumed as high as $tol = 1.0 \cdot 10^{-13}$ for all the cases computed what, for the poorest case, resulted in inaccuracy of the solutions obtained at $\sim 1.6 \cdot 10^{-4}$ as measured by the maximum absolute value of the equation left sides in system (15).

Computing of integrals

All the integrals required in system (15) were calculated numerically as follows. The full distance between the limits of integration was divided into ten equal subintervals. Then, sum of ten resulted integrals calculated each in the range of corresponding subinterval by the Gauss–Legendre ten-point quadrature formula [1] returned the integral in the full range of integration at accuracy estimated as order of $\sim 10^{-8}$ [%].

Computing of derivatives

The first derivatives of each equation with respect to the particular unknowns are required to expand Eqs. (15) into the first order Taylor series. Because of complex forms of the equations the derivatives were calculated numerically. Here, a formula resulted form differentiation of the interpolating Lagrange's polynomial through five equidistant points has been applied to calculate the derivatives at the central point within that five with accuracy for the problem considered order of $\sim 10^{-8}$ [%]. Because the consecutive coefficients (unknowns) keep decreasing values then a number of numerical experiments has been performed as aimed to establish a proper distance between the points for differentiation. In turn, to achieve the assumed accuracy, the points should be separated by 0.01 for the cases with number of trigonometric terms $M \leq 10$ in Eq. (11). If $11 \leq M \leq 21$ the distance was kept decreasingly from 0.001 for $M = 11$ by 10^{-9} for $M = 21$.

Starting guess

The computational strategy developed starts running using initial values (starting guess) for unknowns. Choice of the starting values can be of critical matter for convergence of the iterative process as well as for proper physical meanings of the solutions obtained. Then, particular attention was paid to select a starting guess and many computational trials in this respect were performed also. At first, based on experience gained and rough results presented in [8], as obtained by means of a pocket calculator with the use of the same strategy, a starting guess, was established as follows: $E_1 = 1.0175633$, $C_1 = 0.10668869$, and $C_i = -0.00499$ for $i = 2, \ldots, M$, and verified throughout all the cases computed. The experience gained showed that to achieve the convergence criteria required

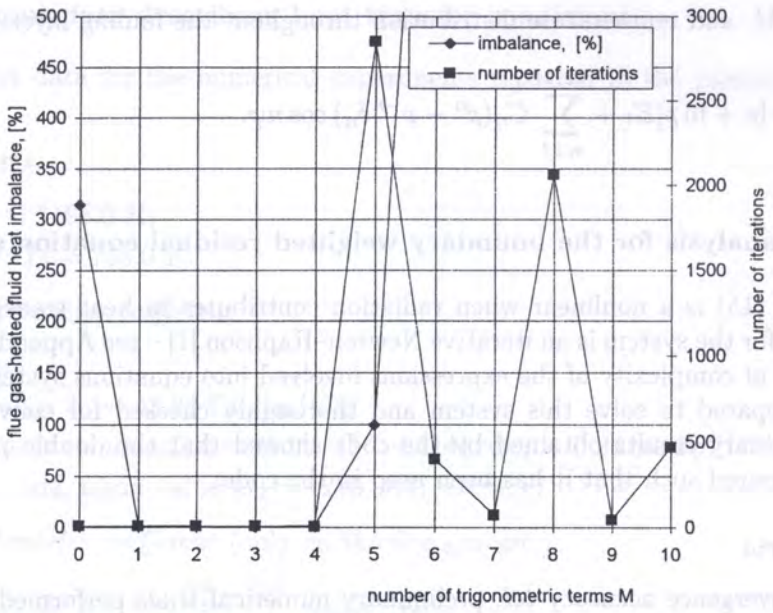

Fig. 3. Improper starting gues – see description in the text, given absolute values of flue gas-heated fluid heat imbalance and number of iterations required for solutions of equations system (15) vs. number of trigonometric terms M, radiation heat transfer mode, fouled tube shown in Fig. 4c

such the starting guess when applied to cases with $M > 4$ can lead to thousands of iterations or to non-physical solutions. Exemplary results are presented in Fig. 3 where it can be seen that:

- a few iterations are required to attain the convergence in region by $M = 4$; however, for larger M values, number of iterations executed to achieve the required convergence does vary randomly from tens up to several thousands,
- as M is up beyond 4 all the results obtained are out of physical sense because imbalance (normalised) $\Delta q = (\dot{Q}_2 - \dot{Q}_1)/\dot{Q}_2$ in the heat rates: $\dot{Q}_1$ as rejected by the hot gas and $\dot{Q}_2$ as absorbed by the cold, increases by unacceptable large values although the iterative process converges, consequently, it means that putative root does exist far away from the starting guess used.

In turn, the most effective starting guess has been found to be as follows: $E_1 = 1.0$, and $C_i = 0.0$ for $i = 1, \ldots, M$. This guess appeared to be effective up to $M = 23$ and was used finally to perform computations throughout all the cases in point.

4.3. Results of the numerical experiments

In this section, to illustrate testing of the algorithm with respect to convergence and accuracy, results of systematic series of numerical experiments are shown. The experiments were performed using a specific input data set given in Section 4.1 and the same starting guess as the above mentioned throughout all the experiments. To emphasise practical significance of the method, a calculated temperature distribution chart and thermal resistance of the two-dimensional foulant deposits are also presented.

4.3.1. Illustrative results for convergence and accuracy

Several levels for testing of the algorithm developed with respect to its convergence and accuracy were implemented and three cases have been established to be used in the experiments related to. The first two are: a case of the clean tube and case of uniform deposit thickness, each selected

for testing or comparison purposes. The third is a case of nonuniform shape of the fouling layer deposited on the tube of the same dimensions as the former two. Also each case of the fouled tube is featured by the same properties and amount of the foulant as well as the convection heat transfer coefficient and absorption/emission properties for radiative heat transfer. In Fig. 4 schematics of assumed shapes of the fouling layer are depicted accompanied by relevant dimensions.

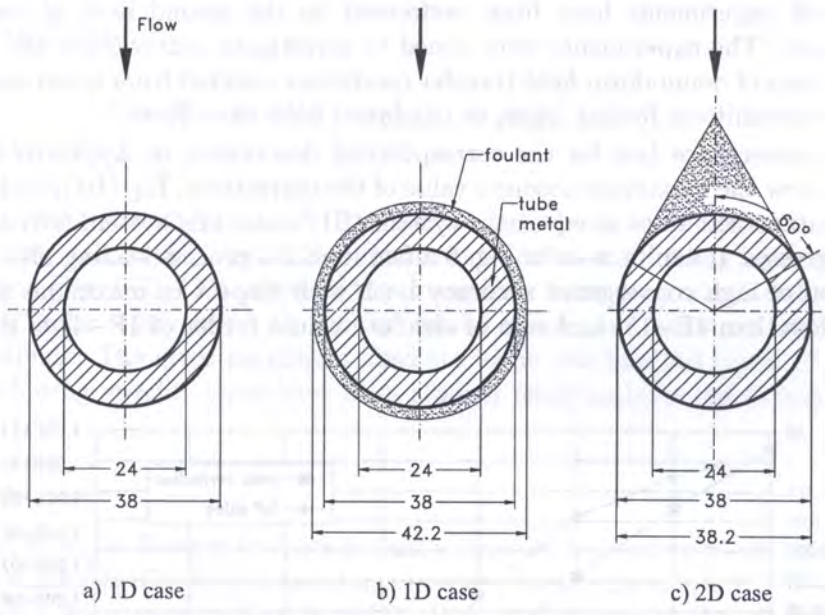

Fig. 4. Clean tube and fouling shapes (either with the same foulant mass) assumed for numerical experiments: a) clean tube, b) uniform fouling deposit, c) nonuniform deposit shape with increased amount of foulant material on forward periphery of the tube

4.3.1.1. Testing with 1D cases

The first test of the lowest level, refers to series of the experiments carried out in order to verify how the algorithm developed can manage 1D cases, as shown in Figs. 4a,b. for which exact solutions can be easily derived, if one assumes a steady heat transmission at constant transfer coefficients across a clean or uniformly fouled tube. Then, as it is well known, the tube wall and fouling layer temperatures depend only on radial coordinate accordingly to the natural logarithm function. Because Eqs. (9) and (10) also involve a term of the *ln* function, then equations system (15) developed with two terms i.e. a *constant* and *ln* function only must provide exact solutions for such the problems. Consequently, results obtained by the Trefftz method and those from exact solutions should be perfectly the same, if one assumes the same computational accuracy requirements. Thus, the exact solutions were derived (when radiation contributes only numerically) for cases presented in Figs. 4a and 4b and resulted temperature distributions computed either for the clean tube wall and, for the fouling layer if the deposit was on, assuming modes of heat transfer as pure convection, pure radiation and combined convection and radiation modes. The comparisons of the accurate results with those obtained from the algorithm and code based on the Trefftz method confirmed that at least six significant digits are identical (note: the single precision was used in the code while testing 1D cases).

More, also correctness of trends in the solutions obtained with respect to identified dependency on the co-ordinates has been verified. Here, for 1D cases, as the above mentioned, the temperature distributions do not depend on the angular coordinate. Then, all such the cases were deliberately recalculated with $M \geq 1$ on input to the code in order to check magnitudes of the computed coefficients, assisting the trigonometric terms in Eqs. (10) and (16), expecting that the coefficient values on the output should be negligibly small. The results obtained confirmed that the code works

as desired because coefficients A_n, B_n and C_n where $n = 1, \ldots, 9$, were correctly of very small values of order max $\sim 3.8 \cdot 10^{-17}$. Consequently, the wall and foulant temperature distributions computed by the algorithm for all 1D cases studied appeared to be independent on the angular coordinate.

4.3.1.2. Testing with 2D cases

Series of numerical experiments have been performed on the second level of verification of the algorithm developed. The experiments were aimed to investigate convergence and accuracy of the solutions for 2D cases of nonuniform heat transfer conditions resulted from either nonuniform transfer coeffcients, or nonuniform fouling layer, or combined both the effects.

In Fig. 5 the convergence (see for the corresponding description in Appendix B) is illustrated where it is shown how the maximum absolute value of the corrections, Eq. (B4), and sum of absolute values of the equations left sides in equations system (B1) emboding system (15) are decreasing as the iterating progresses. It can be seen in Fig. 5 a fast iterative process leading after eight iterations done to a solution of high convergence accuracy both with respect to maximum absolute value of the corrections (less than 1E−15) and sum of absolute values (order of 1E−4) of the equations left sides.

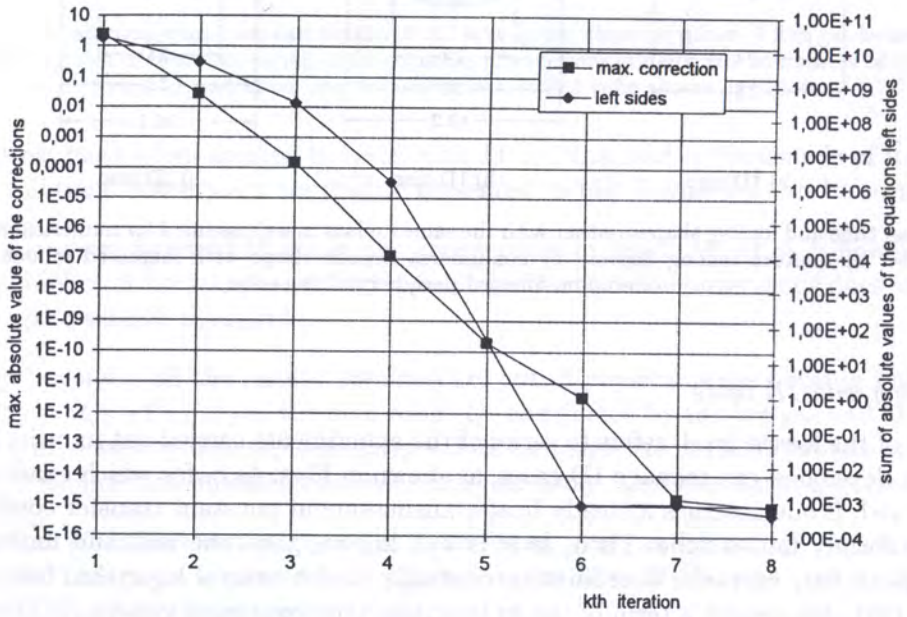

Fig. 5. Convergence of the iterative process (see a description in Appendix B) for solving of equations system (15) developed with $M = 20$ (21 unknowns) vs. number of iterations performed for convection and radiation heat transfer modes combined, fouled tube shown in Fig. 4c

However, the approach applied to analyse the model equations provides solutions that satisfy boundary conditions in approximate manner. Thus, series of the experiments were carried out as aimed to determine how errors in boundary conditions (3)–(6) and number of iterations executed for the convergence depend on number of trigonometric terms M in equations system (15), keeping the same starting guess as already established and $tol = 1.0 \cdot 10^{-13}$. The errors studied were defined as

- for boundary condition (3):

$$\Delta_3 = \left.\frac{\partial \theta_m}{\partial \rho}\right|_{\rho=1} - Bi_2\, \theta_m|_{\rho=1}\,, \tag{17}$$

- for boundary conditions (4) and (5):

$$\Delta_4 = \theta_m|_{\rho=\rho_o} + \Theta_2 - \Theta_1\,\theta_f|_{\rho=\rho_o}\,, \tag{18}$$

$$\Delta_5 = \left.\frac{\partial\theta_m}{\partial\rho}\right|_{\rho=\rho_o} - k\Theta_1 \left.\frac{\partial\theta_f}{\partial\rho}\right|_{\rho=\rho_o}\,, \tag{19}$$

- for boundary condition (6):

$$\Delta_6 = \left.\frac{\partial\theta_f}{\partial N}\right|_{\Gamma_f} + \frac{1}{\rho_o}\left[Bi_c\theta_f + Bi_r\theta_f^4\right]\Big|_{\Gamma_f} - \frac{1}{\rho_o}[Bi_c + Bi_r]\,, \tag{20}$$

where boundary temperatures θ_m and θ_f required in the above definitions are calculated using assumed approximate solutions (10) and (11) for the tube metal and fouling layer temperatures, respectively. Based on Eqs. (17)–(20) values of the errors have been determined as locally distributed along a boundary under study using 19 equally spaced points, by increment 10° with respect to the angular coordinate. The error maximum absolute value was selected using 19 local values determined. The following specific cases have been studied using transfer conditions as presented in Section 4.1.

Convection transfer mode

Heat is transferred from the flue gas to outer foulant surface by convection mode solely, such that the convection heat transfer coeffcient is nonuniform, as described in Section 4.1. The results obtained for the case in point are shown in Figs. 6 and 7. As it can be seen in Fig. 6 distributions of the boundary errors determined at $M = 20$ are such that the following observations can be reported:

- for conditions (3)–(5) values of the errors are small to be within bounds: −8.26E−16 and 7.38E−16,
- for condition (6) values of the errors are within bounds: −1.52E−3 and 1.31E−3.

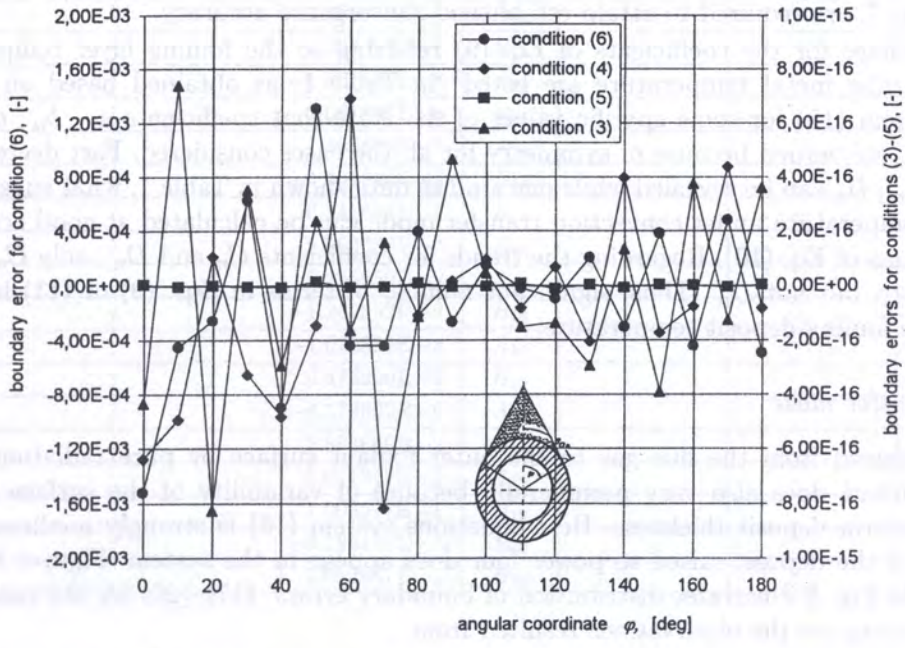

Fig. 6. Distribution of the boundary errors for conditions (3)–(6) at number of trigonometric terms $M = 20$, convection heat transfer mode – fouled tube shown in Fig. 4c

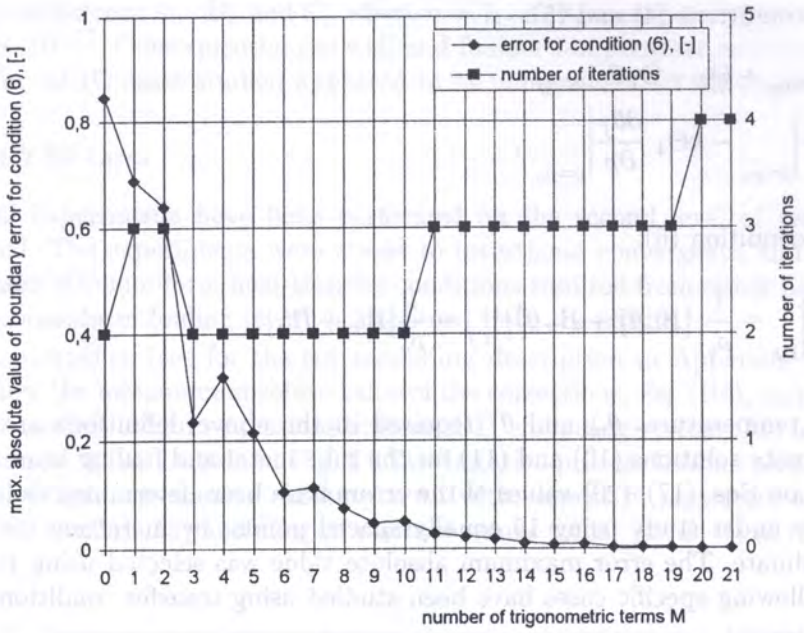

Fig. 7. Maximum value of boundary error of condition (6) and number of iterations required for solutions of equations system (15) vs. number of trigonometric terms M for convection heat transfer mode – fouled tube shown in Fig. 4c

Throughout $M = 0$ by $M = 21$ boundary errors (17)–(19) related to conditions (3)–(5) are very small, thus not shown on a chart – maximum absolute value of the errors Δ_3, Δ_4 and Δ_5 is not greater than 1.01E−15. In turn, one can see that boundary conditions (3)–(5) can be regarded as perfectly satisfied and critical for accuracy of the approach applied are boundary errors of condition (6) – see in Fig. 7. From Fig. 7 it can be concluded that maximum absolute value of the boundary errror Δ_6 for condition (6) essentialy depends on number of the trigonometric terms M and decreases with increasing M such that starting from $M = 0$ the error is ~ 0.85 falling down to ~ 0.0016 when $M = 21$. Regarding the iterative process, it converges very fast and a few iterations only – see Fig. 7, are required to attain established convergence accuracy.

Final outcomes for the coefficients of Eq. (9) referring to the fouling layer temperature, and Eq. (10) for tube metal temperature are listed[1] in Table 1, as obtained based on solutions of equations system (15) for some specific values of M. Note that coefficients a_n, b_n, c_n, d_n where $n = 1, \ldots, M$, are zeroed because of symmetry for all the cases considered. Fast decreasing trends in values of A_n, B_n can be revealed while one studies data shown in Table 1, what suggests that the metal tube temperature under convection transfer mode can be calculated at good accuracy using only a few terms of Eq. (10). Regarding the trends for coefficients C_n and D_n, only C_n values drop down essentialy, but not D_n. Thus, significant number of terms in Eqs. (9) or (11) is required to determine the fouling deposit temperature.

Radiation transfer mode

Heat is transferred from the flue gas to the outer foulant surface by pure radiation mode. The transfer coefficient does also vary peripherally because of variability of the surface temperature due to nonuniform deposit thickness. Here equations system (15) is strongly nonlinear as surface temperature of the deposit raised to power four does appear in the system. Figures 8 and 9 refer to the case. As Fig. 8 illustrates distribution of boundary errors (17)–(20) for the case in point at $M = 20$, following are the observations resulted from:

[1]Outcomes for the coefficients were obtained using double precision Fortran and such are available form the Author on a request, values presented in Tables 1–3 are rounded to seven significant digits.

Table 1. Values of the coefficients in Eqs. (9) and (10) determined for $M = 5$, 10 and 20, convection heat transfer mode at the outer foulant boundary, fouled tube shown in Fig. 4c

Eq. (9) for θ_f	$M = 5$	$M = 10$	$M = 20$	Eq. (10) for θ_m	$M = 5$	$M = 10$	$M = 20$
E_0	6.054098E−2	6.846835E−2	6.943803E−2	F_0	1.394351E−2	1.375310E−2	1.372981E−2
E_1	1.285224	1.267673	1.265526	F_1	3.073556E−2	3.031585E−2	3.026451E−2
C_1	1.929521E−2	1.228958E−2	1.131120E−2	A_1	7.974947E−4	5.079433E−4	4.675059E−4
D_1	−4.776200E−2	−3.042075E−2	−2.799895E−2	B_1	−2.997281E−4	−1.909040E−4	−1.757061E−4
C_2	−1.136333E−2	−8.999918E−3	−8.874621E−3	A_2	−5.348079E−4	−4.235756E−4	−4.176785E−4
D_2	7.021880E−2	5.561430E−2	5.484004E−2	B_2	2.598699E−5	2.058207E−5	2.029553E−5
C_3	−1.673868E−2	−1.359869E−2	−1.332965E−2	A_3	−8.014278E−4	−6.510890E−4	−6.382076E−4
D_3	2.591513E−1	2.105374E−1	2.063721E−1	B_3	−1.225340E−4	−9.954799E−5	−9.757851E−5
C_4	−4.198984E−3	−3.320384E−3	−3.188745E−3	A_4	−2.005692E−4	−1.586019E−4	−1.523140E−4
D_4	1.629886E−1	1.288847E−1	1.237749E−1	B_4	−5.805074E−5	−4.590414E−5	−4.408424E−5
C_5	1.445246E−3	−4.268113E−4	−4.392672E−4	A_5	6.880158E−5	−2.031855E−5	−2.091152E−5
D_5	−1.406535E−1	4.153793E−2	4.275016E−2	B_5	2.669924E−5	−7.884845E−6	−8.114954E−6
C_6		1.662703E−4	9.914509E−5	A_6		7.899354E−6	4.710294E−6
D_6		−4.056946E−2	−2.419111E−2	B_6		3.654628E−6	2.179213E−6
C_7		1.442138E−4	1.010303E−4	A_7		6.844548E−6	4.795011E−6
D_7		−8.821680E−2	−6.180109E−2	B_7		3.566212E−6	2.498343E−6
C_8		3.213805E−5	3.907564E−5	A_8		1.524598E−6	1.853711E−6
D_8		−4.928513E−2	−5.992424E−2	B_8		8.659228E−7	1.052848E−6
C_9		−2.441294E−5	6.214555E−6	A_9		−1.157888E−6	2.947520E−7
D_9		9.385647E−2	−2.389209E−2	B_9		−7.022909E−7	1.787751E−7
C_{10}		2.405210E−6	−2.493411E−6	A_{10}		1.140674E−7	−1.182503E−7
D_{10}		−2.318159E−2	2.403168E−2	B_{10}		7.286255E−8	−7.553445E−8
C_{11}			−2.232540E−6	A_{11}			−1.058745E−7
D_{11}			5.394295E−2	B_{11}			−7.052563E−8
C_{12}			−7.485178E−7	A_{12}			−3.549665E−8
D_{12}			4.534012E−2	B_{12}			−2.447956E−8
C_{13}			−1.361735E−8	A_{13}			−6.457659E−10
D_{13}			2.067845E−3	B_{13}			−4.585218E−10
C_{14}			1.208835E−7	A_{14}			5.732555E−9
D_{14}			−4.601898E−2	B_{14}			4.172941E−9
C_{15}			6.143694E−8	A_{15}			2.913469E−9
D_{15}			−5.863330E−2	B_{15}			2.166895E−9
C_{16}			5.223950E−9	A_{16}			2.477306E−10
D_{16}			−1.249852E−2	B_{16}			1.877370E−10
C_{17}			−1.079832E−8	A_{17}			−5.120789E−10
D_{17}			6.476800E−2	B_{17}			−3.945248E−10
C_{18}			−4.379062E−9	A_{18}			−2.076642E−10
D_{18}			6.584609E−2	B_{18}			−1.623518E−10
C_{19}			2.671319E−9	A_{19}			1.266795E−10
D_{19}			−1.006977E−1	B_{19}			1.003416E−10
C_{20}			−3.188192E−10	A_{20}			−1.511907E−11
D_{20}			3.012887E−2	B_{20}			−1.211723E−11

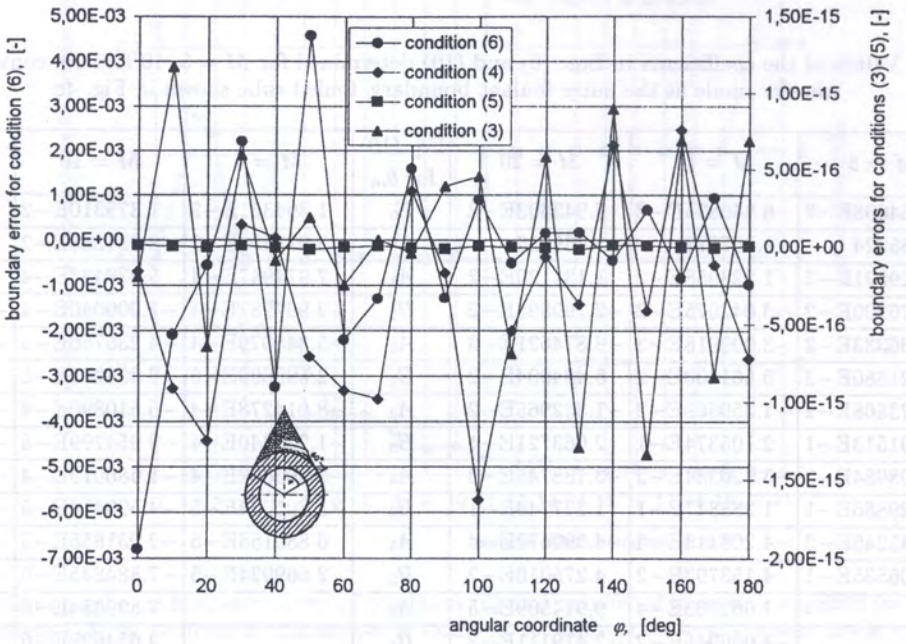

Fig. 8. Distribution of the boundary errors for conditions (3)–(6) at number of trigonometric terms $M = 20$, pure radiation heat transfer mode at foulant outer periphery, fouled tube shown in Fig. 4c

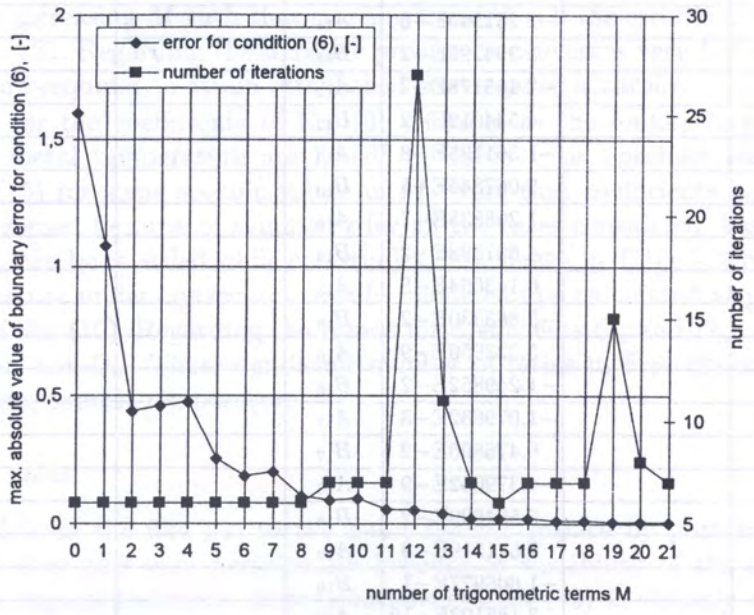

Fig. 9. Maximum value of boundary error for condition (6) and number of iterations required for solutions of equations system (15) vs. number of trigonometric terms M, pure radiation heat transfer mode at foulant outer periphery, fouled tube shown in Fig. 4c

Table 2. Values of the coefficients in Eqs. (9) and (10) determined for $M = 5$, 10 and 20, radiation heat transfer mode at the outer foulant boundary, fouled tube shown in Fig. 4c

Eq. (9) for θ_f	$M = 5$	$M = 10$	$M = 20$	Eq. (10) for θ_m	$M = 5$	$M = 10$	$M = 20$
E_0	−5.081594E−1	−5.014744E−1	−4.995335E−1	F_0	2.760294E−2	2.744238E−2	2.739576E−2
E_1	2.544263	2.529463	2.525167	F_1	6.084494E−2	6.049101E−2	6.038825E−2
C_1	−2.177342E−1	−2.217982E−1	−2.236830E−1	A_1	−8.999222E−3	−9.167191E−3	−9.245092E−3
D_1	5.389639E−1	5.490236E−1	5.536891E−1	B_1	3.382242E−3	3.445371E−3	3.474649E−3
C_2	−6.006145E−2	−5.643063E−2	−5.611641E−2	A_2	−2.826755E−3	−2.655873E−3	−2.641084E−3
D_2	3.711452E−1	3.487088E−1	3.467670E−1	B_2	1.373556E−4	1.290522E−4	1.283336E−4
C_3	−1.865545E−2	−1.579455E−2	−1.524142E−2	A_3	−8.932005E−4	−7.562236E−4	−7.297407E−4
D_3	2.888271E−1	2.445340E−1	2.359704E−1	B_3	−1.365655E−4	−1.156225E−4	−1.115734E−4
C_4	−3.533061E−3	−3.609331E−3	−3.364874E−3	A_4	−1.687606E−4	−1.724037E−4	−1.607270E−4
D_4	1.371400E−1	1.401005E−1	1.306116E−1	B_4	−4.884439E−5	−4.989881E−5	−4.651922E−5
C_5	1.895314E−3	−2.284344E−4	−2.732787E−4	A_5	9.022731E−5	−1.087473E−5	−1.300956E−5
D_5	−1.844549E−1	2.223159E−2	2.659591E−2	B_5	3.501374E−5	−4.220062E−6	−5.048509E−6
C_6		3.762699E−4	2.385880E−4	A_6		1.787625E−5	1.133510E−5
D_6		−9.180874E−2	−5.821476E−2	B_6		8.270430E−6	5.244175E−6
C_7		2.419097E−4	1.646759E−4	A_7		1.148131E−5	7.815705E−6
D_7		−1.479783E−1	−1.007337E−1	B_7		5.982101E−6	4.072214E−6
C_8		3.529591E−5	5.689767E−5	A_8		1.674404E−6	2.699171E−6
D_8		−5.412785E−2	−8.725511E−2	B_8		9.510076E−7	1.533042E−6
C_9		−5.357553E−5	6.620236E−6	A_9		−2.541050E−6	3.139931E−7
D_9		2.059732E−1	−2.545175E−2	B_9		−1.541216E−6	1.904454E−7
C_{10}		7.684065E−6	−5.475525E−6	A_{10}		3.644176E−7	−2.596774E−7
D_{10}		−7.405958E−2	5.277352E−2	B_{10}		2.327782E−7	−1.658735E−7
C_{11}			−4.224347E−6	A_{11}			−2.003326E−7
D_{11}			1.020693E−1	B_{11}			−1.334465E−7
C_{12}			−1.416367E−6	A_{12}			−6.716779E−8
D_{12}			8.579387E−2	B_{12}			−4.632093E−8
C_{13}			−5.155217E−9	A_{13}			−2.444722E−10
D_{13}			7.828386E−4	B_{13}			−1.735859E−10
C_{14}			2.784843E−7	A_{14}			1.320633E−8
D_{14}			−1.060158E−1	B_{14}			9.613378E−9
C_{15}			1.486878E−7	A_{15}			7.051090E−9
D_{15}			−1.419025E−1	B_{15}			5.244254E−9
C_{16}			9.413159E−9	A_{16}			4.463916E−10
D_{16}			−2.252137E−2	B_{16}			3.382877E−10
C_{17}			−3.073392E−8	A_{17}			−1.457466E−9
D_{17}			1.843411E−1	B_{17}			−1.122887E−9
C_{18}			−8.973527E−9	A_{18}			−4.255432E−10
D_{18}			1.349311E−1	B_{18}			−3.326896E−10
C_{19}			6.620525E−9	A_{19}			3.139590E−10
D_{19}			−2.495663E−1	B_{19}			2.486838E−10
C_{20}			−8.346711E−10	A_{20}			−3.958183E−11
D_{20}			7.887760E−2	B_{20}			−3.172300E−11

- for conditions (3)–(5) values of the errors are small to be between −1.63E−15 and 1.17E−15,
- for condition (6) values of the errors are between: −6.79E−3 and 4.58E−3.

Throughout $M = 0$ by $M = 21$ maximum absolute values of boundary errors (17)–(19) referred to conditions (3)–(5) appeared to be very small again not exceeding 1.66E−15. Thus, similar as it is for convection mode, boundary conditions (3)–(5) at the radiation mode are satisfied accurately and critical for accuracy of the approach applied are boundary errors of condition (6). From Fig. 9 it can be concluded that maximum absolute value of boundary error of condition (6) essentially depends on number of the trigonometric terms M and decreases with increasing M such that starting from $M = 0$ the error is ∼1.60 falling down to ∼0.0054 when $M = 21$.

A few iterations are required to attain the convergence in region by $M = 11$. For larger M values, required number of iterations can vary more randomly jumping up to max. 27 when $M = 12$. Consequently, it means that targeted root for the case in point can be reached fast because it does exist not far away from the starting guess established.

Regarding the coefficients of Eq. (9), and Eq. (10) for the radiation mode, these are listed in Table 2, for some specific values of M. Again fast decreasing trends in values of A_n , B_n are selfevident what indicates that good accuracy for the metal tube temperature distributions calculated can be assured with only a few terms of Eq. (10). Behaviour of coefficients C_n and D_n is similar as for the former case. Thus, also for radiation mode significant number of terms of Eqs. (9) or (11) must be taken into account to if one wishes to determine the fouling deposit temperature at reasonable accuracy.

Convection and radiation transfer modes

Heat is transferred from the flue gas flowing over the tube to the outer foulant surface by convection and radiation modes combined. Both the heat transfer coefficients are nonuniform. Here equations system (15) is nonlinear, as for the former case, due to involving the radiation transfer. The results obtained from numerical experiments for the case in point are shown in Figs. 10, 11 and 12.

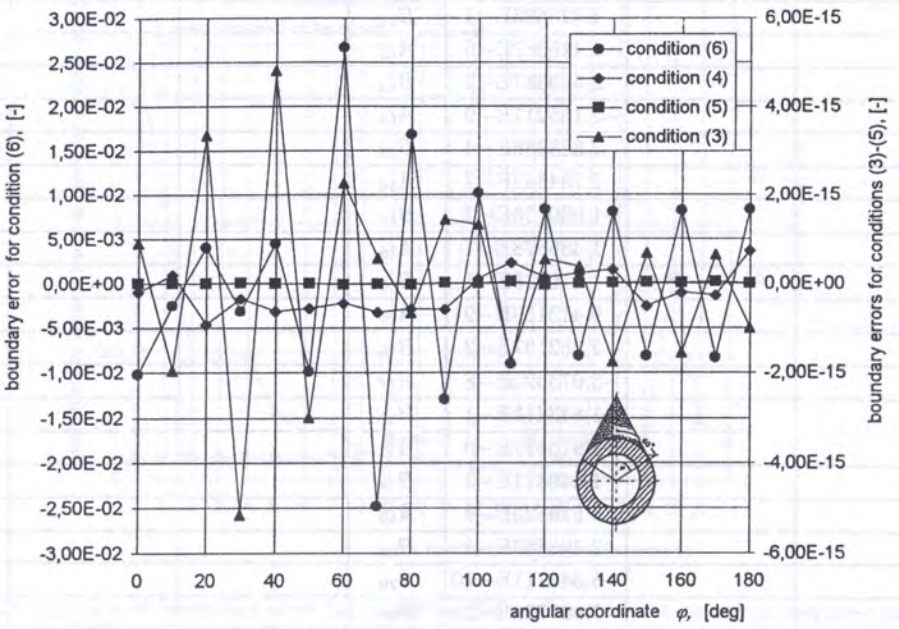

Fig. 10. Distribution of the boundary errors for conditions (3)–(6) at number of trigonometric terms $M = 20$, convection and radiation heat transfer mode at the foulant outer periphery, fouled tube shown in Fig. 4c

As Fig. 10 illustrates distribution of the boundary errors (17)–(20) at $M = 20$, following is the summary:

- for conditions (3)–(5) values of the errors Δ_3, Δ_4 and Δ_5 range from −5.15E−15 to 4.80E−15,
- for condition (6) values of the error Δ_4 range from −2.48E−2 to 2.67E−2.

Then, by examining the above data it can be concluded that the biggest values of the boundary errors refer to condition (6), as it was noted for both the former cases studied. Regarding boundary errors for conditions (3)–(5), these throughout $M = 0$ by $M = 21$ are again very small such that maximum absolute value of the errors is not greater than 5.31E−15. Thus, boundary conditions (3)–(5) can be also regarded as perfectly satisfied at the convection and radiation modes combined and critical for the accuracy are boundary errors of condition (6). Given in Fig. 11 the maximum absolute value of boundary error (20) related to condition (6) continuously decreases with increasing M values such that at $M = 0$ the error is ~2.65 and decreases to ~0.0165 when $M = 21$.

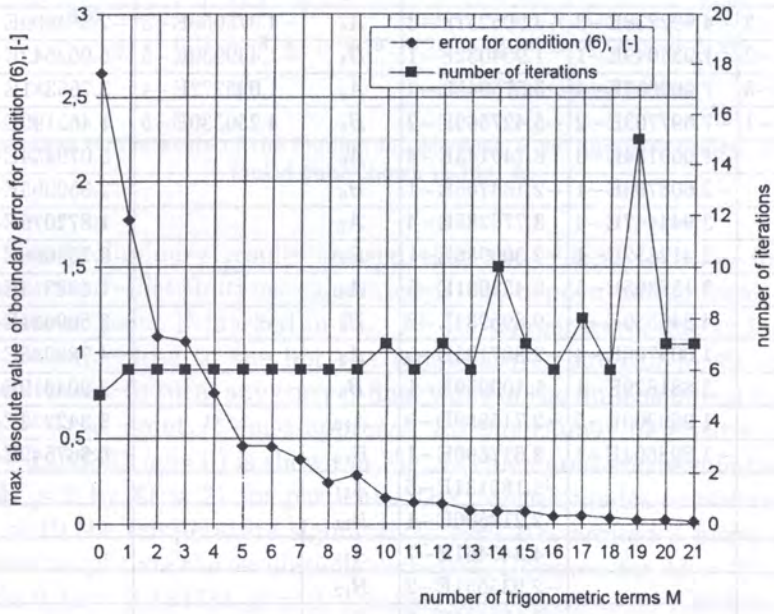

Fig. 11. Maximum value of boundary error for condition (6) and number of iterations required for solutions of equations system (15) vs. number of trigonometric terms M, convection and radiation heat transfer mode at the foulant outer periphery, fouled tube shown in Fig. 4c

A few iterations – see Fig. 11, are required to attain the convergence in region by $M = 9$. For larger M values, required number of iterations can vary more randomly up to max. 15. In turn, it means that the starting guess established correctly identifies that putative root exists somewhere nearby in the neighbourhood.

The coefficients of Eq. (9), and Eq. (10) for the case in point are displayed in Table 3. Again fast decreasing trends in values of A_n, B_n occur what indicates that good accuracy for the metal tube temperature distributions calculated can be assured with only a few terms in Eq. (10). Behaviour of coefficients C_n and D_n is similar as for the former case. Thus, also for combined radiation and convection modes Eqs. (9) or (11) must be computed with significant number of terms to obtain good accuracy in the fouling deposit temperature determined.

Temperature distribution chart

To prepare a temperature distribution chart some preliminary calculations were performed. These were aimed to establish a proper number M of trigonometric terms in order to get the final outcomes

Table 3. Values of the coefficients in Eqs. (9) and (10) determined for $M = 5$, 10 and 20, radiation and convection heat transfer modes at the outer foulant periphery combined, fouled tube shown in Fig. 4c

Eq. (9) for θ_f	$M = 5$	$M = 10$	$M = 20$	Eq. (10) for θ_m	$M = 5$	$M = 10$	$M = 20$
E_0	−8.903542E−1	−8.937868E−1	−8.917214E−1	F_0	3.678276E−2	3.686521E−2	3.681560E−2
E_1	3.390400	3.398000	3.393427	F_1	8.107994E−2	8.126168E−2	8.115233E−2
C_1	−3.369786E−1	−3.258063E−1	−3.272656E−1	A_1	−1.392774E−2	−1.346597E−2	−1.352629E−2
D_1	8.341331E−1	8.064779E−1	8.100901E−1	B_1	5.234562E−3	5.061013E−3	5.083681E−3
C_2	−9.396524E−2	−8.780289E−2	−8.697516E−2	A_2	−4.422416E−3	−4.132389E−3	−4.093432E−3
D_2	5.806510E−1	5.425712E−1	5.374563E−1	B_2	2.148908E−4	2.007980E−4	1.989050E−4
C_3	−3.004568E−2	−3.042550E−2	−2.972792E−2	A_3	−1.438550E−3	−1.456736E−3	−1.423337E−3
D_3	4.651726E−1	4.710531E−1	4.602530E−1	B_3	−2.199466E−4	−2.227271E−4	−2.176205E−4
C_4	−1.041545E−3	−4.992888E−3	−4.905251E−3	A_4	−4.975056E−5	−2.384909E−4	−2.343048E−4
D_4	4.042880E−2	1.938049E−1	1.904032E−1	B_4	−1.439930E−5	−6.902642E−5	−6.781485E−5
C_5	2.300728E−3	7.909557E−4	5.576945E−4	A_5	1.095272E−4	3.765381E−5	2.654930E−5
D_5	−2.239104E−1	−7.697703E−2	−5.427569E−2	B_5	4.250330E−5	1.461199E−5	1.030276E−5
C_6		1.069154E−3	8.749143E−4	A_6		5.079454E−5	4.156640E−5
D_6		−2.608703E−1	−2.134765E−1	B_6		2.350005E−5	1.923065E−5
C_7		3.944447E−4	3.776285E−4	A_7		1.872079E−5	1.792267E−5
D_7		−2.412852E−1	−2.309986E−1	B_7		9.754086E−6	9.338243E−6
C_8		−3.158395E−5	6.452981E−5	A_8		−1.498313E−6	3.061233E−6
D_8		4.843539E−2	−9.895933E−2	B_8		−8.509931E−7	1.738681E−6
C_9		−1.009700E−4	−2.887105E−5	A_9		−4.788935E−6	−1.369334E−6
D_9		3.881829E−1	1.109959E−1	B_9		−2.904619E−6	−8.305383E−7
C_{10}		1.969900E−5	−2.715989E−5	A_{10}		9.342272E−7	−1.288060E−6
D_{10}		−1.898604E−1	2.617690E−1	B_{10}		5.967542E−7	−8.227715E−7
C_{11}			−9.182131E−6	A_{11}			−4.354472E−7
D_{11}			2.218600E−1	B_{11}			−2.900623E−7
C_{12}			4.845461E−7	A_{12}			2.297843E−8
D_{12}			−2.935051E−2	B_{12}			1.584662E−8
C_{13}			2.151844E−6	A_{13}			1.020454E−7
D_{13}			−3.267654E−1	B_{13}			7.245664E−8
C_{14}			9.593825E−7	A_{14}			4.549598E−8
D_{14}			−3.652261E−1	B_{14}			3.311822E−8
C_{15}			−5.965135E−8	A_{15}			−2.828793E−9
D_{15}			5.692919E−2	B_{15}			−2.103917E−9
C_{16}			−2.595607E−7	A_{16}			−1.230891E−8
D_{16}			6.210098E−1	B_{16}			−9.328027E−9
C_{17}			−5.191448E−8	A_{17}			−2.461893E−9
D_{17}			3.113814E−1	B_{17}			−1.896734E−9
C_{18}			7.524358E−8	A_{18}			3.568207E−9
D_{18}			−1.131406	B_{18}			2.789623E−9
C_{19}			−1.788974E−8	A_{19}			−8.483684E−10
D_{19}			6.743689E−1	B_{19}			−6.719842E−10
C_{20}			1.334059E−9	A_{20}			−8.483684E−10
D_{20}			−1.260705E−1	B_{20}			5.070301E−11

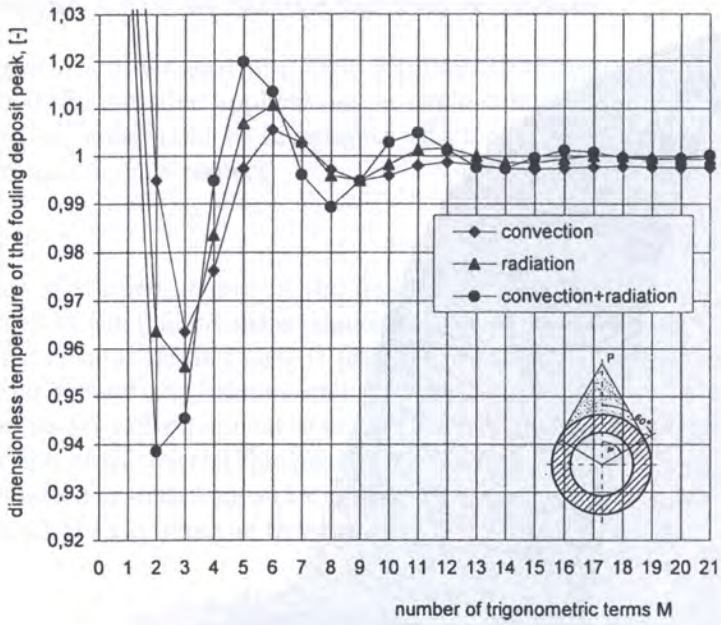

Fig. 12. Dimensionless temperature of the fouling deposit peak P vs. number of trigonometric terms M, fouled tube shown in Fig. 4c

of good accuracy. The preliminary results showed that the critical location for accuracy of the fouling deposit temperature distributions calculated is the deposit corner peak located at $\varphi = 0$ and $\rho = 3.183333$ – see at point P marked in Fig. 12. Its temperature, due to low deposit thermal conductivity, must be very close to the hot gas temperature, but can never exeed it as heat is transported into the deposit. In turn, any correct final value of the dimensionless fouling temperature $\theta_f(\rho = 3.183333, \varphi = 0)$ at point P must approach 1.0 but cannot be greater than or equal 1.0. Temperature $\theta_f(\rho = 3.183333, \varphi = 0)$ is shown in Fig. 12 calculated versus number of trigonometric terms throughout $M = 0$ by $M = 21$ for particular the transfer modes considered. One can see in Fig. 12 that by $M = 10$ the temperature significantly oscillates around 1 being greater or smaller than 1. As M increases amplitude the oscillations decreases. However, for $M = 20$ and $M = 21$ under the convection mode $\theta_f(\rho = 3.183333, \varphi = 0)$ remains unchanged to be 0.99758 what corresponds to 1195.1K as correct value of the temperature calculated. Similiarly, for the radiation mode the result is perfect also as the temperature is 0.99933 what gives 1197.2 K of the dimensional peak temperature. At last, when both the modes are employed the ratio is 0.99950, thus, the temperature is 1197.4 K. Finally, a spatial temperature distribution chart as demonstrated here in Fig. 13 was computed with number of the terms $M = 20$. Due to be abilities of a software being at disposal, the chart was prepared using the cartesian coordinate system.

The chart displays temperature difference $T - T_2$ throughout the whole domain considered consisting the fouling layer and tube metal. Note in the chart the predominant effect of the fouling deposit thermal resistance and hardly perceptible influence of heat conduction across the tube metal. In turn, the surface showing temperature distribution in the circular region of the tube metal is very flat and the surface goes up rapidly in fouling deposit at the close vicinity of the tube metal where the corresponding temperature gradients are extremely strong. This surface becomes flattened in further regions of the deposit such that the deposit peak at $\varphi = 0$ and $\rho = 3.183333$, piercing upward the flue gas flow – see Fig. 4c is almost adiabatic as being at temperature of 1197.4 K vs. 1198.0 K of the flue gas inflowing on. Small steep peaks seen at the outer backward periphery of the tube result from the use of the cartesian coordinates and illustrate the temperature distribution along lines $x = \text{const}$ and $y = \text{const}$ passing the thin circular fouling layer of thickness 0.1 mm deposited around the backward side of the tube – see a schematics of the fouled tube shown in Fig. 4c.

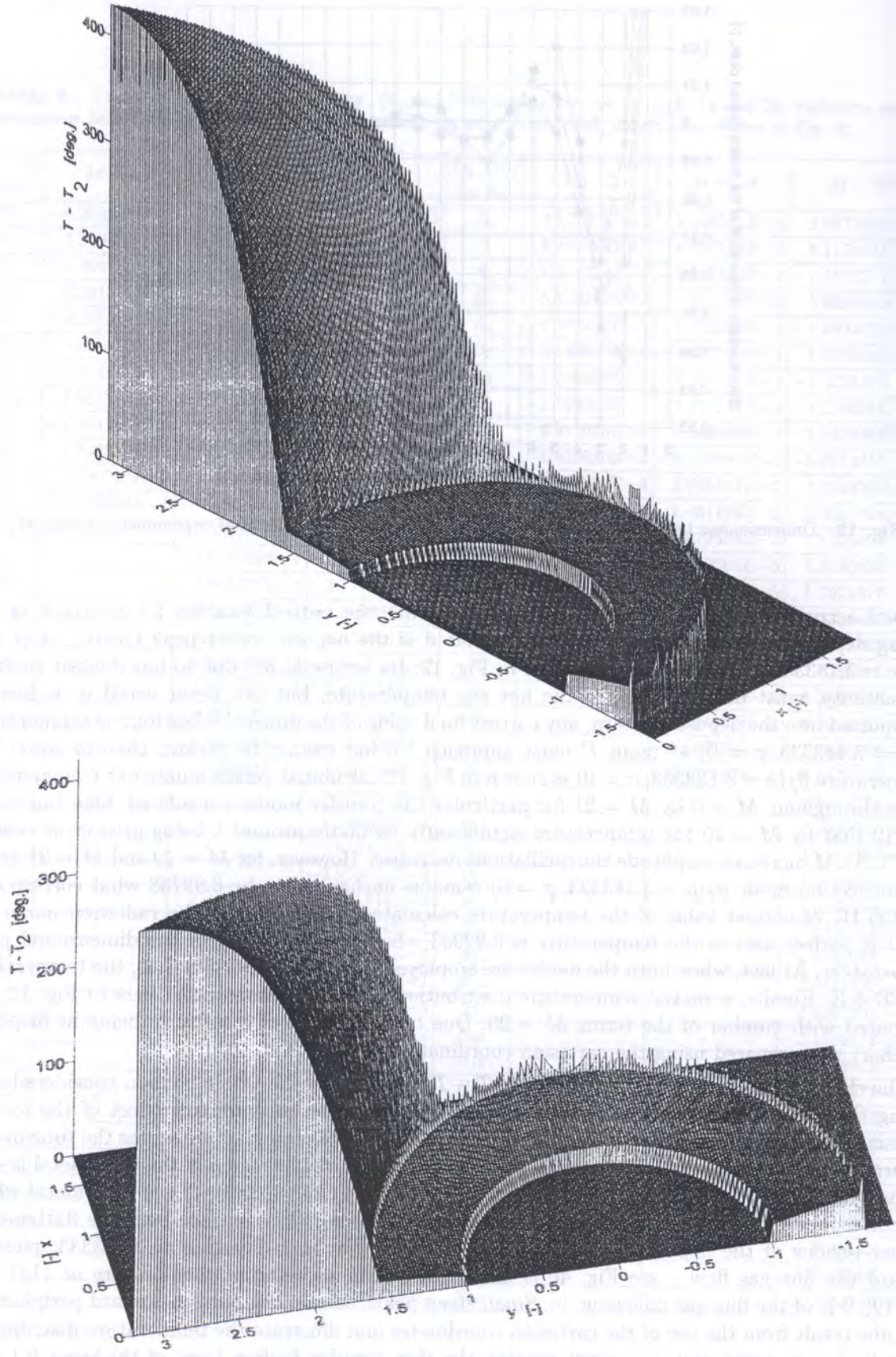

Fig. 13. Temperature distribution across the fouled tube calculated with $M = 20$, convection and radiation heat transfer modes at the foulant outer periphery combined, fouled tube dimensions are shown in Fig. 4c

4.3.2. Effect of fouling shape on fouling thermal resistance

The aim of this section is to demonstrate some representative results, obtained by means of the methodology described, for possible applications in engineering. Consequently, outcomes from numerical experiments [12], conducted to investigate effect of fouling deposit shape on its thermal resistance, have been used in this respect.

Fouling shapes studied

In Fig. 14 schematics of studied shapes of the fouling layer are depicted in a systematic manner with increasing amount of the foulant mass deposited on forward periphery of the tube and accompanied by relevant dimensions. Either case is featured by the same properties and amount of the foulant mass deposited around the tube as well as convection heat transfer coefficient and absorption/emission properties for radiative heat transfer. Note in Fig. 14, the symmetry of fouled tubes with respect to direction of the overall flue gas flow. Then, coefficients a_n, b_n, c_n for $n = 1, \ldots, M$. vanish and Trefftz equation system is given by equations system (15). Assumed input data describing heat transfer conditions are the same as those presented in Section 4.1.

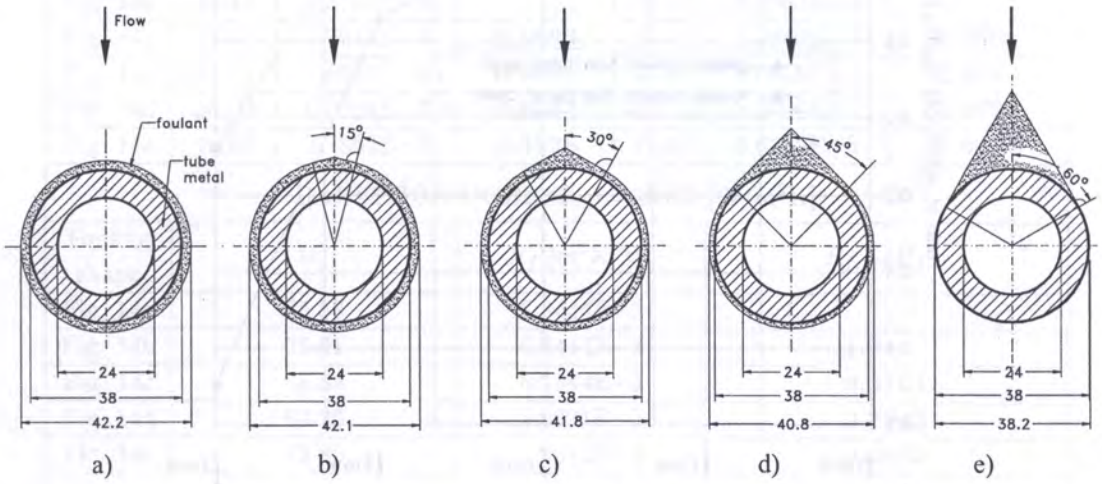

Fig. 14. Fouling shapes (either with the same foulant mass) assumed for the investigation: a) reference case of uniform thickness, b) – e) shapes of nonuniform thickness set up systematically from left to right with increasing amount of foulant on forward periphery of the tube

Determining of the fouling thermal resistance

The procedure applied to determine the fouling thermal resistance consists in the following consecutive steps:

- solving equations system (15) for coefficients E_1, C_n, $n = 1, \ldots, M$, either for clean/fouled tube wall,
- calculations all the remaining coefficients E_0, D_n, F_0, F_1, A_n, B_n, $n = 1, \ldots, M$, (formulae are given in Appendix A)
- calculations of, either for fouled/clean tube wall:

heat rate transferred: $\dot{Q} = 2 \int_0^{\pi} \alpha_2 \left(T_m|_{r=r_2} - T_2\right) r_2 \, \mathrm{d}\varphi$, and

overall heat transfer coeffcient: $U = \dfrac{\dot{Q}}{2\pi r_o (T_1 - T_2)}$,

- calculation of the fouling thermal resistance using the following equation,

$$R_f = \frac{1}{U_f} - \frac{1}{U_{cl}} . \tag{21}$$

Fouling thermal resistance vs. fouling shape

To find out how the deposit shape affects its thermal resistance the results obtained are compared: i.e. resistance $R_{f,N}$ for nonuniform deposit of Figs. 14b–e to resistance $R_{f,U}$ for a reference case of the uniform thickness as in Fig. 14a. Consequently Figs. 15–17 present ratio $R_{f,N}/R_{f,U}$ vs. the shapes (see also tabulated results in Table 4) set up systematically from left to right with increasing amount of foulant mass on the forward periphery of the tube.

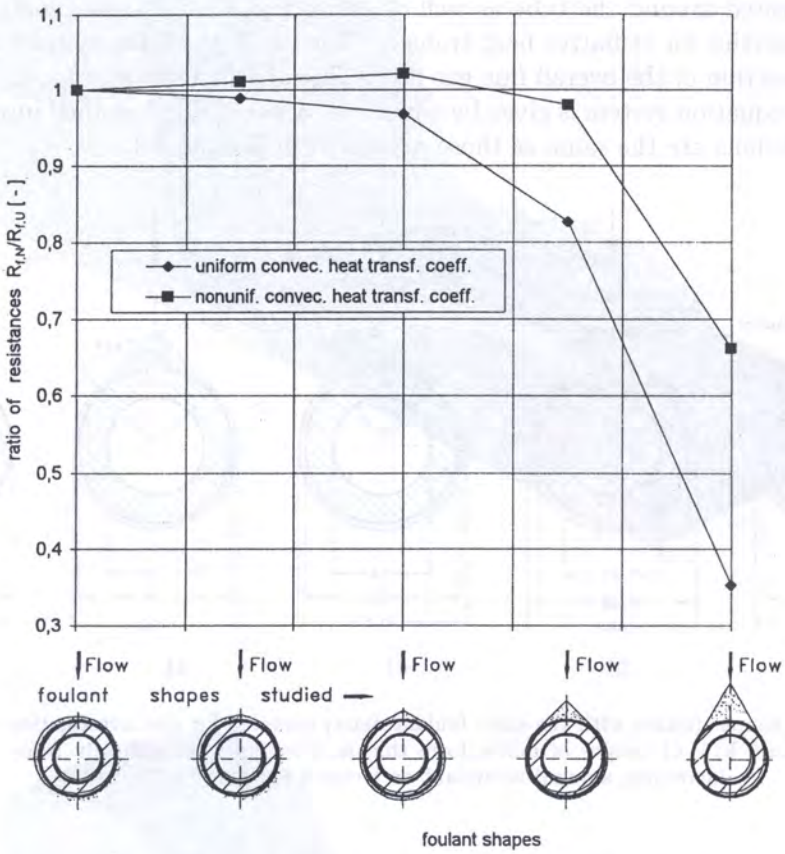

Fig. 15. Ratio of the thermal resistances, nonuniform to uniform fouling layers (either with constant mass of foulant deposited on the same tube), vs. foulant shape, convection mode of heat transfer

The following observations can be made for the results of Figs. 15–17. For all the modes of heat transfer (convection, radiation and combined both) there are significantly strong influence of deposit shape on the fouling thermal resistance. It does mean that the contribution of the fouling resistance decreases in the path of heat flow as the fouling layer becomes more nonuniform. In turn, the highest fouling thermal resistance is for case of the uniform foulant thickness when the foulant deposited significantly insulates all around the tube heat transfer surface area against heat flow. The numerical experiments carried out provided the following particular results. As amount of the foulant mass deposited on forward periphery of the tube increases (from left to right in each figure – see underneath the charts), keeping the deposit mass around the tube at constant, the fouling thermal resistance decreases such that:

- for convection mode, see trends shown in Fig. 15, when foulant shape changes from that of uniform shown in Fig. 14a throughout Figs. 14b,c,d up to the most nonuniform as given in

Table 4. Thermal resistance of nonuniform fouling layers determined in the study [12]

CONVECTION MODE						
Uniform heat transfer coefficient U_{cl}= 47.18, [W/m^{2}K]				Nonuniform heat transfer coefficient U_{cl} = 47.05, [W/m^{2}K]		
Fouling shape	U_f	R_f [m^{2}K/W]	$R_{f,N}/R_{f,U}$	U_f	R_f	$R_{f,N}/R_{f,U}$
Fig. 14a	34.43	7.8752E−3		33.59	8.5061E−3	
Fig. 14b	34.45	7.7910E−3	**0.9893**	33.53	8.5949E−3	**1.010**
Fig. 14c	34.72	7.6239E−3	**0.9681**	33.38	8.6843E−3	**1.021**
Fig. 14d	36.05	6.5063E−3	**0.8262**	33.77	8.3300E−3	**0.9793**
Fig. 14e	41.82	2.7863E−3	**0.3538**	37.18	5.6259E−3	**0.6614**
RADIATION MODE, U_{cl} = 86.62, [W/m^{2}K]						
Fouling shape	U_f		R_f [m^{2}K/W]	$R_{f,N}/R_{f,U}$		
Fig. 14a	55.88		6.3444E−3			
Fig. 14b	55.91		6.3444E−3	**1.0**		
Fig. 14c	56.54		6.1544E−3	**0.9701**		
Fig. 14d	60.26		5.0391E−3	**0.7943**		
Fig. 14e	73.89		1.9871E−3	**0.3132**		
CONVECTION and RADIATION MODES, combined						
Uniform convection heat transfer coefficient U_{cl} =129.33, [W/m^{2}K]				Nonuniform convection heat transfer coefficient U_{cl} =129.21, [W/m^{2}K]		
Fouling shape	U_f	R_f [m^{2}K/W]	$R_{f,N}/R_{f,U}$	U_f	R_f [m^{2}K/W]	$R_{f,N}/R_{f,U}$
Fig. 14a	63.86	7.9155E−3		63.71	7.95	
Fig. 14b	63.89	7.9155E−3	**1.0**	63.69	7.9586E−3	**1.0**
Fig. 14c	64.96	7.6507E−3	**0.9665**	64.55	7.7399E−3	**0.9725**
Fig. 14d	71.34	6.2913E−3	**0.7948**	70.33	6.4848E−3	**0.8148**
Fig. 14e	104.16	1.8630E−3	**0.2354**	99.43	2.3204E−3	**0.2916**

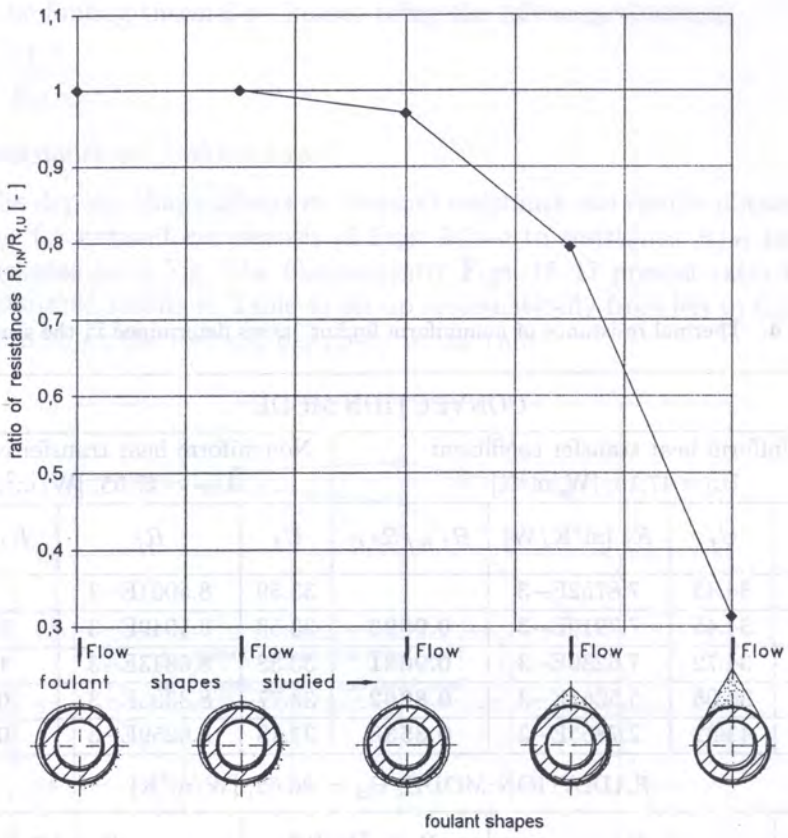

Fig. 16. Ratio of the thermal resistances, nonuniform to uniform fouling layers (either with constant mass of foulant deposited on the same tube), vs. foulant shape, radiation mode of heat transfer

Fig. 14e, the resistance drops by about 65% for the case of uniform heat transfer coefficient, and when the heat transfer coefficient is nonuniform the drop is noteworthy also, however smaller to be about 35%,

- for radiation mode of heat transfer, see the results given in Fig. 16, the resistance drops by about 70% when the foulant takes a shape of nonuniform as given in Fig. 14e, instead of that uniform shown in Fig. 14a,
- for convection and radiation modes combined, see the curves illustrated in Fig. 17, the effect of foulant shape is the strongest such that when the foulant is of nonuniform deposit, shown in Fig. 14e, the resistance even drops by 70–80% of that uniform (shown in Fig. 14a). Also worthy to mention in Fig. 17 is negligible difference between cases of nonuniform and uniform convection heat transfer coefficient.

Such a beneficial effect of the nonuniform deposit shape for mitigation in the fouling thermal resistance is the most probably due to as follows.

As the fouling layer tends to be more nonuniform in shape (keeping the foulant mass unchanged), then thickness of the fouling layer on the forward fraction of the transfer surface area increases, however, on the remaining fraction the thickness decreases – compare dimensions of the layers in Fig. 14a and e.g. in Fig. 14c.

At first, such the modification does not affect essentially the fouling thermal resistance as far as the thickening portion of the layer is not enough thick and the thinning portion is not sufficiently thin to cause a marked change in the resistance – note trends in Figs. 15–17 for the first three shapes starting from the uniform layer settled at the left side in each figure. One can see that the effect studied is yet negligibly small.

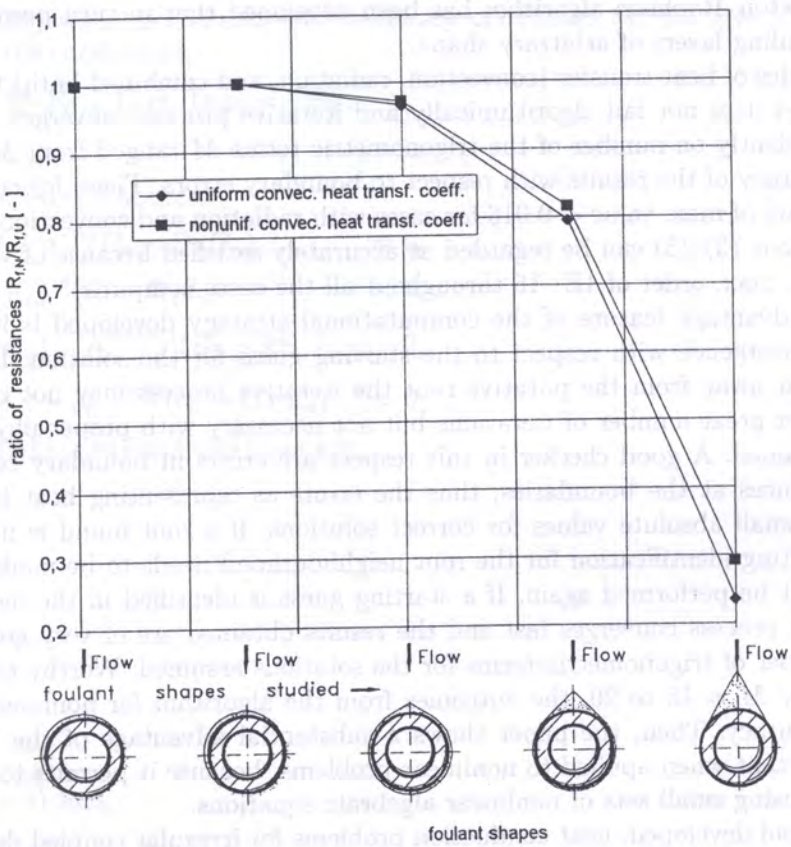

Fig. 17. Ratio of the thermal resistances, nonuniform to uniform fouling layers (either with constant mass of foulant deposited on the same tube), vs. foulant shape, convection and radiation modes combined

Further increase in the foulant mass deposited on the forward periphery of the tube brings about that the foulant covers this portion of the periphery with thicker and thicker layer. Because the whole foulant mass has been assumed to be conserved, therefore, to balance such the increase, the layer deposited on the remaining backward periphery of the tube becomes thinner. In turn, the fouling mass concentrates on a decreasing part of the periphery. When the layer on the forward periphery attains enough thickness it becomes almost a perfect insulator against heat flow due to low foulant thermal conductivity and the outer surface temperature of the layer on this part approaches the flue gas temperature. Consequently, further increase in the foulant mass deposited on the forward periphery does have negligible influence on heat rate transferred across this part of the transfer surface because the surface temperature there, although being closer and closer as the deposit growths, can never overcome the gas temperature.

However, thanks to that, fouling on the remaining portion reduces because the portion is covered with thinner and thinner layer of the foulant. In this manner the portion becomes cleaner and takes increasing fraction of the periphery. In turn, the total thermal resistance in the path of heat flow across the fouled tube decreases – compare results shown in Figs. 15–17 for the uniform deposit (left side) and the most nonuniform layer (right side).

5. Concluding remarks

Comprehensive two-dimensional model of heat transmission process across a nonuniformly fouled tube wall is presented. Based on the variational principle and Trefftz method the boundary weighted residual approach has been developed for analysis of the problem under study. To solve the corresponding nonlinear equation system resulted from, a computational iterative startegy of analysis

based on the Newton–Raphson algorithm has been developed that in turn permits to study heat transfer across fouling layers of arbitrary shape.

For all the modes of heat transfer (convection, radiation, and combined both) the computational strategy developed does not fail algorithmically and iterative process converges at the established accuracy independently on number of the trigonometric terms M ranged from $M = 0$ by $M = 21$. Note perfect accuracy of the results with respect to boundary errors. These for condition (6) calculated at $M = 21$ are of max. value ~ 0.016 for cases with radiation and convection modes combined. Boundary conditions (3)–(5) can be regarded as accurately satisfied because of very small the corresponding errors, max. order of 1E−15 throughout all the cases computed.

The main disadvantage feature of the computational strategy developed is its significant sensitivity of the convergence with respect to the starting guess for the solution. If a starting guess used does exist far away from the putative root the iterative process may not converge at all, or may converge after great number of iterations but not necessary with proper physical meanings of the solutions obtained. A good checker in this respect are errors in boundary conditions as these express heat balances at the boundaries, thus the errors as representing heat imbalances should have sufficiently small absolute values for correct solutions. If a root found is not that desired it means that a starting identification for the root neighbourhood needs to be modified and the iterative process must be performed again. If a starting guess is identified in the neighbourhood of a root, the iterative process converges fast and the results obtained are of very good accuracy even with a small number of trigonometric terms for the solutions assumed. Worthy to mention is that, if one uses already $M = 15$ to 20, the outcomes from the algorithm for nonlinear cases appeared to be of high accuracy. Then, the paper shows a substantial advantage of the Trefftz approach, particularly important when applied to nonlinear problems, because it permits to perform analysis at high accuracy using small sets of nonlinear algebraic equations.

Based on the tool developed, heat conduction problems for irregular coupled domains with presence of huge and small temperature gradients can be effectively studied delivering outcomes of high accuracy. In this respect, a 3D temperature distribution chart across two coupled regions of tube metal with fouling deposit on is presented in the paper. In turn, the chart shows that subtlet temperature trends and differences between the transfer modes can be grasped by the approach.

More, systematic investigations the influence of nonuniform foulant shape on the fouling thermal resistance have been carried out for a specific data set describing heat transfer conditions at a fouled boiler tube. The results of genuine character with respect to the thermal resistance are compared with reference to uniform fouling layer around the tube. The study demonstrates a significant effect of the deposit shape that can reduce the resistance by order of 35%–80%. Although, to apply effectively the method presented, the foulant shapes must be known in advance, the paper clearly elucidates significance of the deposit form for its thermal resistance.

ACKNOWLEDGEMENT

Author gratefully acknowledges the partial financial support for this work by Committee for Scientific Research (KBN, Poland) under the Rector's Grant of Białystok Technical University No. W/WM/5/99.

APPENDIX A

This Appendix demonstrates expressions relating coefficients in Eq. (10) to coefficients in Eq. (9). By substitution Eq. (10) into boundary condition (3) one obtains

$$Bi_2 F_0 - F_1 = 0, \tag{A1}$$

$$A_n(Bi_2 - n) + B_n(Bi_2 + n) = 0, \tag{A2}$$

$$a_n(Bi_2 - n) + b_n(Bi_2 + n) = 0. \tag{A3}$$

Equations (9)–(10) when introduced into boundary conditions (4)–(5) give the following relationships between the coefficients,

$$F_0 + F_1 \ln\rho_0 - \Theta_1 E_0 - E_1\Theta_1 \ln\rho_0 = -\Theta_2\,, \tag{A4}$$

$$F_1 = k\Theta_1 E_1\,, \tag{A5}$$

and the application establishes also

$$\rho_0^n(A_n - \Theta_1 C_n) + \rho_0^{-n}(B_n - \Theta_1 D_n) = 0, \tag{A6}$$

$$\rho_0^n(a_n - \Theta_1 c_n) + \rho_0^{-n}(b_n - \Theta_1 d_n) = 0, \tag{A7}$$

$$\rho_0^{n-1}(A_n - k\Theta_1 C_n) - \rho_0^{-(n+1)}(B_n - k\Theta_1 D_n) = 0, \tag{A8}$$

$$\rho_0^{n-1}(a_n - k\Theta_1 c_n) - \rho_0^{-(n+1)}(b_n - k\Theta_1 d_n) = 0. \tag{A9}$$

Based on Eqs. (A1), (A4) and (A5) one gets

$$F_0 = k\frac{\Theta_1}{Bi_2}E_1\,, \tag{A10}$$

$$F_1 = F_0\,Bi_2\,, \tag{A11}$$

$$E_0 = \Theta + \kappa E_1\,, \tag{A12}$$

where

$$\Theta = \frac{\Theta_2}{\Theta_1}\,, \tag{A13}$$

$$\kappa = \frac{k}{Bi_2} + (k-1)\ln\rho_0\,. \tag{A14}$$

From Eqs. (A6) and (A8) the relations between the coefficients A_n, B_n, C_n and D_n are obtained as

$$A_n = C_n\frac{\Theta_1(1+k)}{2} + D_n\frac{\Theta_1(1-k)}{2\rho_0^{2n}}\,, \tag{A15}$$

$$B_n = C_n\frac{\Theta_1\rho_0^{2n}(1-k)}{2} + D_n\frac{\Theta_1(1+k)}{2}\,. \tag{A16}$$

By applying Eqs. (A7) and (A9) one gets resulting expressions for the coeffcients a_n and b_n as dependent on coefficients c_n and d_n, then

$$a_n = c_n\frac{\Theta_1(1+k)}{2} + d_n\frac{\Theta_1(1-k)}{2\rho_0^{2n}}\,, \tag{A17}$$

$$b_n = c_n\frac{\Theta_1\rho_0^{2n}(1-k)}{2} + d_n\frac{\Theta_1(1+k)}{2}\,. \tag{A18}$$

Combining now Eqs. (A15)–(A16) with Eq.(A2) one obtains

$$D_n = -\delta_n C_n\,, \tag{A19}$$

where

$$\delta_n = \frac{(1+k)(Bi_2-n) + \rho_0^{2n}(1-k)(Bi_2+n)}{(1-k)(Bi_2-n)\rho_0^{-2n} + (1+k)(Bi_2+n)}\,. \tag{A20}$$

Similarly, relation (A3) with the use Eqs. (A17) and (A18) can be written as

$$d_n = -\delta_n c_n\,. \tag{A21}$$

Finally, substituting now Eqs. (A12), (A19) and (A21) into Eq. (9) yields

$$\theta_f(\rho,\varphi) = \Theta + [\kappa + \ln\rho]E_1 + \sum_{n=1}^{n=M}(\rho^n - \rho^{-n}\delta_n)(C_n\cos n\varphi + c_n\sin n\varphi). \tag{A22}$$

APPENDIX B

In this Appendix the iterative Newton–Raphson method is only shortly outlined, as commonly well known for analysis of nonlinear equation systems.

For general case of a nonlinear equation system the problem to be solved can be symbolically written as

$$\left.\begin{aligned} f_1(X_1,\ldots,X_{M+1}) &= 0 \\ f_2(X_1,\ldots,X_{M+1}) &= 0 \\ &\vdots \\ f_{40}(X_1,\ldots,X_{M+1}) &= 0 \end{aligned}\right\} \quad \text{or} \quad \mathbf{f(X)=0}, \tag{B1}$$

where each function $f_i(X_1,\ldots,X_{M+1})$, for $i=1,\ldots,M+1$ corresponds to individual the ith equation in system (24) and contains variables that are just the unknowns $X_1,\ldots,X_{M+1}$, i.e. E_1 and C_n, $n=1,\ldots,M$. Applied here method of solving is an iterative Newton–Raphson [6] that uses the consecutive expansion of equation system (B1) in the first order Taylor series with a starting guess for the solution X_0. Denoting by $\mathbf{X}$ the vector of X_j values, where $i=1,\ldots,M+1$, the expansion of the ith function of system (B1) in Taylor series in the neighbourhood $\mathbf{X}_0$ of the starting guess $\mathbf{X}_0$ gives

$$f_i(\mathbf{X}) = f_i(\mathbf{X}_0) + \sum_{j=1}^{M+1} \frac{\partial f_i(\mathbf{X}_0)}{\partial X_j}\,\delta X_{j,0} + R(\delta \mathbf{X}_0^2) + \cdots$$

where $\delta\mathbf{X}_0 = \mathbf{X} - \mathbf{X}_0$. Neglecting terms of order $\delta\mathbf{X}_0^2$ and higher in the series, and taking into account that according to equation system (B1) each function $f_i(X_1,\ldots,X_{M+1})$ should be zeroed, one obtains a set of linear equations with respect to $\mathbf{X}_0$. Solution of this system yields the vector of corrections $\delta\mathbf{X}_0$ for the $\mathbf{X}_0$ that move all the functions closer to zero simultaneously after the first iteration. As a result on stage of the kth iteration one obtains a set of linear equations written in the matrix notation as

$$\mathbf{A}_k\,\delta\mathbf{X}_k = -f(\mathbf{X}_k), \tag{B2}$$

where the matrix $\mathbf{A}_k$ consists of the first derivatives of each equation in system (B1) with respect to variables $\mathbf{X}$, say on the kth current iteration,

$$\mathbf{A}_k = \left[\frac{\partial f_i(\mathbf{X})}{\partial X_j}\right]_{\mathbf{X}=\mathbf{X}_k}. \tag{B3}$$

Solution of system (B2) yields the vector of corrections $\delta\mathbf{X}_k$ for the $\mathbf{X}_k$ that move all the functions $f(\mathbf{X})$ closer to zero simultaneously. Having in mind that

$$\delta\mathbf{X}_k = [\mathbf{X} - \mathbf{X}_k] \tag{B4}$$

what yields $\mathbf{X}_{k+1} = [\mathbf{X}_k + \delta\mathbf{X}_k]$ as a starting point for the next iteration. Consequently, the expansion about $\mathbf{X}_{k+1}$ is performed now and equation system (B2) with new values of $\mathbf{A}$ and $f(\mathbf{X})$ is solved again. Iterating is continued until a solution satisfies an established convergence accuracy such that the iterative process stops on the k^{th} stage if the maximum absolute value of the corrections $\delta X_{j,k}$, $j=1,\ldots,M+1$, is less than or equal some tolerance tol, thus the convergence accuracy states

$$\max[\mathrm{abs}(\delta X_{j,k})] \le tol, \qquad \text{where} \quad i=1,\ldots,M+1. \tag{B5}$$

Worthy to mention for this work is solving of linear equation system (B2) on each stage of iterating by the LU decomposition method [6].

References

[1] A.F. Gavrilov, B.M. Malkin. *Fouling and Cleaning of Heat Transfer Surfaces in Boilers* (translated, in Russian: А.Ф. Гаврилов, Б.М. Малкин, *Загрязнение и Очистка Поверхностей Нагрева Котельных Установок*). Energija, Moskva, 1980.

[2] A. Kneschke. Berechnung stationarer Temperaturverteilungen. *Ing. Arch.*, **30**: 117–122, 1961.

[3] J. Kołodziej, A. Uściłowska. Trefftz-type procedure for Laplace equation on domains with circular holes, circular inclusions, corners, slits, and symmetry. *CAMES*, **4**(3/4): 501–519, 1997 (Special issue: *1st International Workshop: Trefftz Method – Recent Developments and Perspectives*).

[4] N.V. Kuznetsov. *Operation Processes and Problems of Improvement for Convective Heat Transfer Surfaces in Boilers* (translated, in Russian: Н.В. Кузнецов, *Рабочие Процессы и Вопросы Усовершенствования Конвективных Поверхностей Котельных Агрегатов*). GEI, Moskva, 1958.

[5] A.A. Ots. *Processes in Boilers at Combustion of Bituminous-Estonian-Shales and Kansko-Atchinski Coals* (translated, in Russian: А.А. Отс, *Процессы в Парогенераторах при Сжыгании Сланцев и Канско-Ачинских Углей*). Energija, Moskva, 1977.

[6] W.H. Press, B.P. Flannery, A. Teukolsky, W.T. Vetterling. *Numerical Recipes. The Art of Scientific Computing.* Cambridge University Press, 1986.

[7] W.T. Reid. *External Corrosion and Deposits, Boilers and Gas Turbines.* American Elsevier Publishing, New York, 1971.

[8] T. Skiepko. Temperature field in tube metal of convection surface of steam boiler (in Polish). *Archiwum Energetyki PAN*, No. 4: 227–242, 1980.

[9] T. Skiepko. Variational method of calculation of temperature field in metal tube with an outer fouling layer in a steam boiler (in Polish). *Archiwum Energetyki PAN*, **XIII**(2): 133–144, 1984.

[10] T. Skiepko. A method of calculation temperature distribution in the wall of a boiler tube and an example of its application (in Polish). *Dozór Techniczny*, No. 4: 136–140, 1984.

[11] T. Skiepko. The temperature field in a metal tube with outer fouling layer (in Polish). *Archiwum Termodynamiki*, **7**(2): 148–160, 1986.

[12] T. Skiepko. Fouling shape – yet another factor to mitigate fouling thermal resistance. In: T.R. Bott, A.P. Watkinson, C.B. Panchal, eds., *Mitigation of Heat Exchanger Fouling and Its Economic and Environmental Implications. Proceedings of UEF Conference,* Banff, Canada, 11–16 July, 1999.

[13] E. Trefftz. Ein Gegenstück zum Ritzschen Verfahren. In: *Internat. Kongress fur Technische Mechanik*, Verhanl. d.2: 131–137, Zürich, 1926.

[14] V.M. Zusman, V.V. Tichonova. On formation of ash deposits on tubes made of 12% chromic steels (translated, in Russian: В.М. Зусман, В.В. Тихонова, Об избирательном образовании золовых отложений на трубах из 12%-ных хромистых сталей). *Teploenergetika*, No. 11: 57–61, 1970.